Right-handed Neutrinos from Leptoquark Decays: the Monolepton Channel at the Large Hadron Collider

Thesis submitted in partial fulfillment
of the requirements for the degree of

*Master of Science in **Computational Natural Sciences** by Research*

by

Yash Chaurasia
20171116
yash.chaurasia@research.iiit.ac.in

International Institute of Information Technology
Hyderabad - 500 032, INDIA
October 2023

International Institute of Information Technology
Hyderabad, India

CERTIFICATE

It is certified that the work contained in this thesis, titled "Right-handed Neutrinos from Leptoquark Decays: the Monolepton Channel at the Large Hadron Collider" by Yash Chaurasia, has been carried out under my supervision and is not submitted elsewhere for a degree.

_____ _____

Date Adviser: Dr Subhadip Mitra

To

The Giants Whose Shoulders We Stand Upon

Acknowledgments

First and foremost, I would like to express my sincere gratitude to my advisor, Dr. Subhadip Mitra, for his invaluable guidance and support throughout my Master's journey. He encouraged me to explore everything that intrigued me, be it beyond the scope of our research area. This thesis is a testimony to his superb mentorship. I also thank Dr. Sujit Gujar and Dr. Pawan Kumar for letting me work with them on their area of expertise. These collaborations broadened my knowledge and enriched my research experience.

I feel blessed to have Dr. Arvind Bhaskar as my mentor-cum-friend. He was helpful and empathetic while guiding me and everyone who sought his help. He played the most significant role in the successful completion of my Master's requirements. I am grateful to Cyrin Neeraj for our physics discussions, his valuable feedback and his suggestions.

I am indebted to my parents for their unwavering support in my life and for understanding the struggles associated with research.

I would reminisce about the time spent with my batchmates Prajwal, Tanmay, Siddharth, Pratyush, Sayantan, Rohan and Aditya, having late-night discussions on countless topics which expanded the horizons of my knowledge. I want to thank Yashas and Jayadev for being exemplary role models with honest work ethic. They inspired me to maintain integrity and uphold ethical values even in challenging situations, a crucial aspect of my character development. I feel lucky to have shared my hostel room with Aradhya and Visvesh, with whom I had a pleasant stay. I thank Gaurav, Chaitanya and Parth for the Age of Empires games that helped me get through the COVID lockdown. I thank Ansh for his contributions to the Astronomy Club. I thank Pradeep Pal for encouraging me to play and improve at basketball. I spent time with numerous people post-COVID, too many to acknowledge here. I thank them all for their impact on my campus life.

I am grateful for the diverse opportunities at IIIT that came my way, many of which I utilized to grow as an individual. I am thankful for the trust placed in me through various positions of responsibility and for considering my opinions during administrative decisions.

To all the readers, this QR code links to a media extending this acknowledgement. I hope you like it!

Abstract

The Standard Model of particle physics explains the particle content of matter and their interactions at the fundamental level. While the theory predicts and explains most subatomic events quite accurately, it has some limitations; also, some anomalies have been observed. Consequently, various theories beyond the standard model have been developed. Leptoquarks (LQs) and Right-handed Neutrinos (RHNs) are two hypothetical particles appearing in many of these new theories. They are well-known for their potential to address multiple issues. Experiments at the Large Hadron Collider (LHC) have put bounds on their parameters (if they exist) with certain assumptions. However, no direct experimental constraints exist on Leptoquark (LQ) couplings with quarks and right-handed neutrinos (RHNs) yet. If the RHNs are lighter than the LQs, they can be produced from the LQ decays. This simultaneous probe for RHNs and the LQs that dominantly couple to RHNs has never been searched for in experiments.

In this thesis, we investigate the signals arising from the decays of Right-Handed Neutrinos (RHNs) coming from the decays of a scalar Leptoquark (LQ) that dominantly couples to RHNs. Our investigation covers both pair and single productions of the LQ and also RHN pair production through t-channel LQ exchange. These typically lead to two RHNs which can subsequently decay to multiple charged leptons and jets. While the dilepton final state is the most promising, our analysis centres on the more challenging monolepton final state to compute the discovery and exclusion reach of LQs and RHNs at the LHC. Here, we consider a scalar Leptoquark with an electromagnetic charge of either $1/3$ or $2/3$ (referred to as ϕ_1 and ϕ_2 respectively), primarily coupling to second-generation quarks and RHNs.

We discuss the Standard Model and some Beyond Standard Model theories in chapter 1. We discuss particle accelerators and their simulation software in chapter 2. We analyse the monolepton final state to estimate the discovery reach at the high-luminosity LHC in chapter 3. In chapter 4, we visualise the distributions of various parameters and then look at them collectively to maximise the discovery reach. We present the results of the work in chapter 5.

In chapter 6, we digress from the main topic and study a computation technique that can be used to automatically compute the bounds on LQ parameters from the current LHC data. We discuss an alternative methodology to compute the χ^2 test on a contingency table where the table elements involve couplings as variables. These individual elements are summed up to form polynomials, and the polynomial form of χ^2 is computed. This allows for using computational techniques (like gradient descent) that cannot be utilised if the value of χ^2 is computed using the regular tabular method at discrete values of the couplings.

Contents

List of Figures

List of Tables

Chapter 1

The Theoretical Motivation: the Standard Model and Beyond

As humans, we have evolved to be curious. We have explored and tried to make sense of the world around us for ages. We have uncovered the fundamental laws that govern things that happen through observations and experiments. Our current understanding of the rules that dictate this universe is a culmination of ideas, hypotheses, experiments, coincidences and experiences of millions of people and civilizations which have thrived and perished. We now have a decent understanding of various everyday phenomena, from cloud formation, tides, eclipses, phases of the moon, projectile motion, buoyancy and fluid dynamics to more fundamental laws governing gravity, electromagnetic radiation, the tiny atoms, and even the evolution of the universe itself. These discoveries not only feed our hunger for knowledge but also advance us technologically, making our lives simpler.

We have realized that most phenomena of nature are explainable by a few fundamental laws. We now know of four fundamental forces of nature, namely, 1) *gravitational force*, 2) *electromagnetic force*, 3) *strong force* and 4) *weak force*. Einstein's *General Theory of Relativity* describes the gravitational force. We have achieved the unification of electric, magnetic and weak interactions in the past centuries; the Standard Model of Particle Physics now describes the three fundamental forces (electromagnetic, weak, and strong). However, despite our progress, we still do not understand much about the universe. There are limitations to our technologies, anomalies encountered in experiments, and theoretical limits. We are still far away from a unified "Theory of Everything".

This chapter gives a brief introduction to the Standard Model (SM) of Particle Physics and physics Beyond the Standard Model (BSM).

1.1 Development of the Standard Model

Atomic theories have been around for centuries, mainly as philosophical theories. Stoichiometry was followed by the development of the periodic table, where atoms were believed to be the fundamental particles of nature. In the late 19th century, physicists discovered the atom's negatively charged constituent, the *electron*. Soon, the positively charged nucleus was confirmed. Chemical reactions do not change the nuclei; hence, the elements remain conserved. Radioactive processes modify the nuclei

and change the element from one to another. Also, isotopes were discovered. Thus, the nucleons: 1) *proton* and 2) *neutron* were conjectured and subsequently discovered. Electromagnetic force implies that positively charged protons should strongly repel each other, breaking the nucleus. To explain the stability of the nucleus, nuclear forces were hypothesized.

Further development was facilitated by quantum mechanics, which describes the behaviour of the particles at the subatomic level through the *wave-particle duality* and the *uncertainty principle*. Combining the special theory of relativity and quantum mechanics, quantum field theory was born. Quantum field theory describes particles as excitations of the respective quantum fields. The Standard Model is based on this mathematical framework.

1.2 Particles in the Standard Model

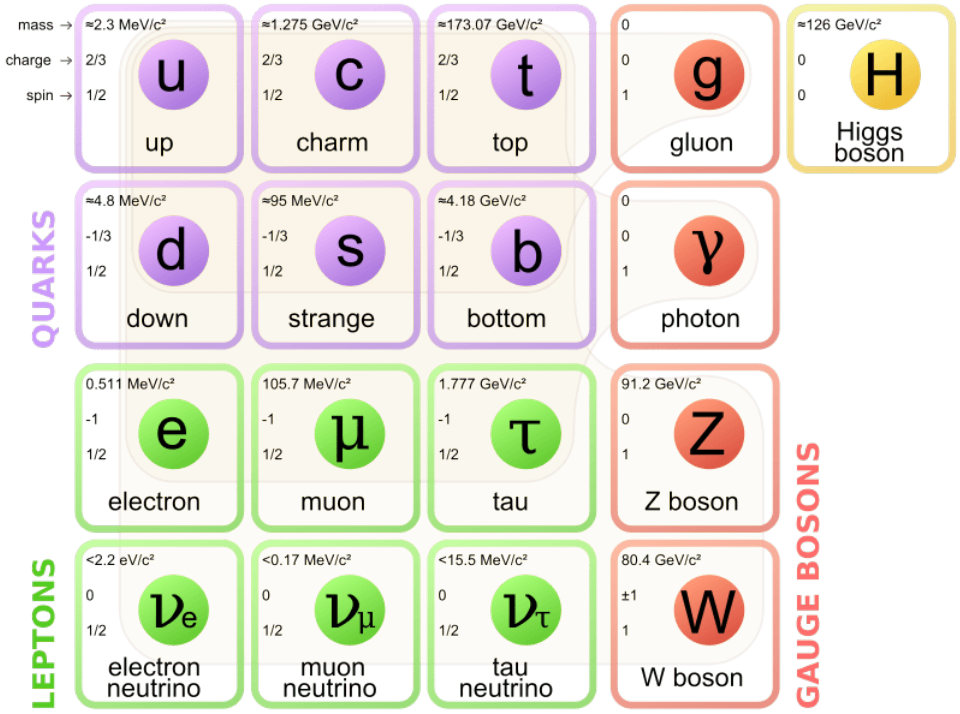

Figure 1.1: The Particles of the Standard Model

The Standard Model of Particle Physics describes the elementary particles and the quantum interactions between them. The elementary particles are divided into two main categories: 1) *fermions*, with half-odd-integer spin and 2) *bosons*, with an integral spin quantum number. Bosons typically transmit forces, and fermions comprise matter. Fermions are further divided into *quarks* and *leptons*. There are three generations of quarks and leptons, with each generation of quarks having an up-type quark and a down-type quark, and each generation of leptons having a charged lepton and a neutral lepton. Thus, there are six *flavours* of quarks and leptons each, making twelve fermions in total. There is one scalar

boson, the *Higgs boson*, and four vector bosons, namely, 1) *photon*, 2) *gluon*, 3) Z *boson* and 4) W *boson*. Higgs boson (H^0) gives the particles their masses via the Higgs mechanism. Photons (γ) are the force carrier of the electromagnetic field. Gluons (g) are the force carriers that mediate the strong force. Z bosons (the neutral weak boson) and $W^{\pm}$ bosons (charged weak bosons) mediate the weak force.

1.2.1 Fermions

Fermions follow the *Fermi-Dirac statistics*, which characterizes a system of non-interacting, identical particles obeying the *Pauli exclusion principle*. Fermions have half-odd-integer spins like spin $\frac{1}{2}$ or spin $\frac{3}{2}$. The Pauli exclusion principle restricts two or more identical half-odd-integer spin particles from simultaneously occupying the same quantum state. There are both elementary and composite fermions. Elementary fermions can be further classified as either quarks or leptons. Composite particles comprising an odd number of elementary fermions are also fermions. Fermions are typically associated with matter, e.g., electrons, protons, and neutrons.

According to the Fermi-Dirac distribution, the probability that a particle will have energy E is given by:

$$f(E) = \frac{1}{e^{(E-E_F)/(k_B T)} + 1}$$

where E_F is the *Fermi Energy*, k_B is the *Boltzmann constant* and T is the temperature.

1.2.1.1 Quarks

Quark	Generation	Charge (e)	Mass ($\times c^{-2}$)
Up (u)	1	+2/3	1.5 - 4 MeV
Down (d)	1	-1/3	4 - 8 MeV
Charm (c)	2	+2/3	1.15 - 1.35 GeV
Strange (s)	2	-1/3	80 - 130 MeV
Top (t)	3	+2/3	169 - 174 GeV
Bottom (b)	3	-1/3	4.1 - 4.4 GeV

Table 1.1: Properties of quarks [1].

Quarks are spin $\frac{1}{2}$ particles with electric charge either $-\frac{1}{3}e$ or $+\frac{2}{3}e$. They possess colour charges and hence engage in strong interactions. They also experience weak interaction and gravity, making them the only elementary particles of the standard model which experience all four fundamental interactions. There are six flavours of quarks; three generations of up-type and down-type quarks. They are: *up*, *down*, *charm*, *strange*, *top*, and *bottom*. For each quark flavour, there is an *antiquark*, the antiparticle of the quark. Thus, a quark and the corresponding antiquark have the same mass, opposite electric charge, opposite colour charge and opposite baryon number. They annihilate after interacting with each other.

Due to *colour confinement*, quarks are not found in isolation. They are trapped inside *hadrons* as *valence quarks* or as *virtual sea quarks*. There are two types of hadrons, namely, *baryons* and *meson*. Baryons are composite subatomic particles with an odd number of valence quarks, more than one, typically three. Thus, baryons are fermions. Protons are baryons with three valance quarks—two up quarks and one down quark (uud), while neutrons contain one up and two down quarks (udd). Mesons are subatomic particles with an equal number of quarks and antiquarks. Thus, mesons are bosons.

1.2.1.2 Leptons

Lepton	Generation	Charge (e)	Mass (MeV/c^2)
Electron (e)	1	-1	0.5110
Electron neutrino (ν_e)	1	0	$< 3 \times 10^{-6}$
Muon (μ)	2	-1	105.658
Muon neutrino (ν_μ)	2	0	0.19
Tau (τ)	3	-1	1777
Tau neutrino (ν_τ)	3	0	< 18.2

Table 1.2: Properties of leptons [1].

Leptons are spin-$\frac{1}{2}$ particles with either $-e$ electric charge or no electric charge. They are fermions that do not take part in strong interactions. There are three generations of leptons, with one charged and one neutral lepton (*neutrino*) in each generation. The six leptons are: *electron*, *electron neutrino*, *muon*, *muon neutrino*, *tauon*, *tau neutrino*. The charged leptons have masses and interact weakly. Thus, they experience three of the four fundamental forces: gravitational force, weak force and electromagnetic force. Neutrinos, on the other hand, possess no mass and no electric charge in the Standard Model. The left-handed neutrinos only experience the weak force, while the Standard Model does not have any right-handed neutrinos. Note that currently, there is some evidence (e.g. 1.4.5) for neutrinos having small masses.

Corresponding to each lepton, there is an antilepton with the same mass but opposite charges. The interaction between a gauge boson and any lepton is flavour-independent. This is known as *lepton universality*. In any system, each generation's *leptonic number* is conserved.

Electron, the lightest charged lepton, is stable, and the heavier charged leptons decay to it. It forms the negatively charged component of an atom, and it is the movement of electrons which generates electricity. Table 1.2 lists the properties of all leptons.

1.2.2 Bosons

Bosons are particles that follow *Bose-Einstein statistics*, which describes how a collection of non-interacting, identical particles occupy available discrete energy states. They are not restricted to single

occupancy of a particular state and, thus, do not obey the Pauli exclusion principle. An unlimited number of bosons can condense at low temperatures into the same energy state, forming the *Bose-Einstein condensate*. Bosons have integer spin values like spin 1 or spin 2. Bosons either act as force carriers between particles or give rise to *mass*. There are categorized based on their spin as scalar or vector bosons.

According to the Bose-Einstein distribution, the number of particles expected in energy state i at temperature T is:

$$n_i = \frac{g_i}{e^{(\epsilon_i - \mu)/(k_B T)} - 1}$$

where ϵ_i is the energy of the i-th state, μ is the chemical potential, k_B is the Boltzmann's constant, g_i is the degeneracy of energy level i and $\epsilon_i > \mu$.

1.2.2.1 Scalar / Higgs Boson

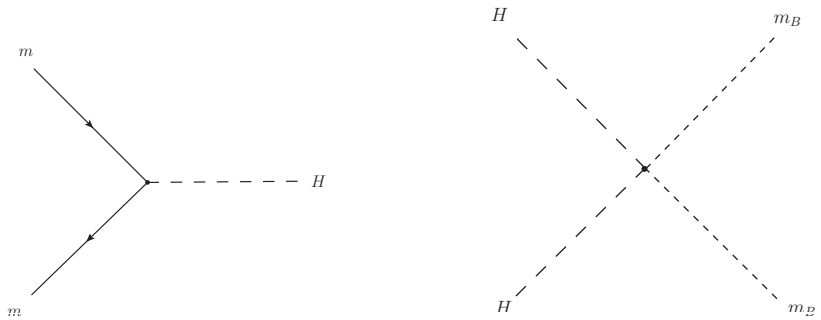

(a) (b)

Figure 1.2: Interaction of the Higgs boson in the Standard Model: m_B represents a boson with a mass and m is any particle with a mass.

The Higgs boson (H^0) is a scalar boson, a spin-0 boson. It is produced by the quantum excitation in the *Higgs Field*. The Higgs field is a scalar field that gives masses to gauge bosons via *electroweak* gauge symmetry breaking and, simultaneously, gives masses to fermions through *Yukawa couplings*. The Higgs boson has no electric charge and no colour charge. It has a mass of around 125 GeV/c^2 and is the last elementary particle of the Standard Model to be discovered in 2012.

1.2.2.2 Gauge Bosons

Gauge Bosons or Vector Bosons are bosons with spin 1. Gauge bosons are quanta of the gauge fields, and the number of gauge bosons of a type is equal to the number of generators of the particular gauge field. They are the force carriers of gauge fields and mediate the interactions between particles that are associated with these fields. Gauge fields have gauge symmetry, which allows any physical system to be described in different ways. We discuss the individual gauge bosons below:

- **Photon**: A photon is a quantum of the electromagnetic field and the force carrier of the electromagnetic force. The gauge group in *quantum electrodynamics* is $U(1)$. There is only one generator, and hence, only one gauge boson, the photon, in quantum electrodynamics. Photons are massless and have no electric charge. They do not have colour charge and do not feel the weak force (they, however, interact with $W^{\pm}$ boson electromagnetically).

  Photons are the particles of electromagnetic radiation, which, depending on their energies, can be classified as visible light, ultraviolet radiation, infrared radiation, etc. Their energy (E) and frequency (ν) are related as $E = h\nu$, where h is the Planck's constant. Photons travel at speed c, that is, at 299,792,458 metres per second. This speed c is also known as the speed of light and is the maximum speed at which any matter, energy or information can travel through space according to the special theory of relativity.

- **Gluon**: Gluons are the gauge bosons that mediate the strong force between quarks in *quantum chromodynamics*. Unlike the photon of the $U(1)$ gauge group, the $SU(3)$ group of quantum chromodynamics has eight generators, and hence, there are eight gluons. Each gluon has a colour and an anticolour. As they themselves have colour charge, they also participate in the strong interaction apart from mediating it, unlike photons. This makes quantum chromodynamics harder to analyse. Gluons are massless particles with no electric charge either. They do not participate in weak interactions.

- **$\mathbf{W^{\pm}}$ and $\mathbf{Z^0}$ boson**: W^+, W^- and Z^0 bosons mediate the weak force. They correspond to the three generators of $SU(2)$ in electroweak theory. W^+ has electric charge $+e$, W^- has electric charge $-e$, and Z^0 boson has no electric charge. All three of them have mass and, thus, interact gravitationally. As they have very high masses, their range of interaction is limited. Only $W^{\pm}$ interacts electromagnetically. W^+ and W^- are antiparticles of each other, whereas Z^0 is its own antiparticle. $W^{\pm}$ bosons have *weak isospin* $(T_3) = \pm 1$, and for Z bosons, $T_3 = 0$. Emission or absorption of Z^0 changes the spin, momentum and energy of the particles, while emission or absorption of $W^{\pm}$ changes the charge by e and type of the particle.

1.3 Fundamental Forces

There are four known fundamental forces in physics. The gravitational force is described by the *general theory of relativity* as an effect of the curvature of *spacetime*, whereas the electromagnetic force, the weak nuclear force, and the strong nuclear force are discrete quantum fields described by the Standard Model. More specifically, the Standard Model is based on a gauge field theory, the *Yang-Mills* theory, with the unitary product group being:

$$\underbrace{SU(3)}_{\text{Strong interaction}} \times \underbrace{SU(2) \times \quad \underbrace{U(1)}_{\text{Electromagnetism}}}_{\text{Electroweak interaction}}$$

Fermions are particles of matter, and bosons are considered force carriers as fermions do not interact directly with each other but exchange virtual gauge bosons. These virtual bosons are not the same as the stable, on-shell particles that can be directly observed. They result from the uncertainty principle and affect other particles, leading to observable effects. The interactions are constrained by the conservation of various properties like electric charge, colour charge, momentum, flavour, etc. Gravity and electromagnetic force can be felt at large scales. The strong nuclear force and the weak nuclear force only operate at subatomic distances. We discuss these interactions in detail below.

1.3.1 Electromagnetic Force

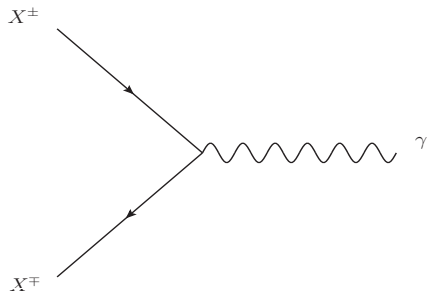

Figure 1.3: A basic QED (quantum electrodynamics) vertex. Here $X^{\pm}$ represents any charged particle in the Standard Model. γ represents a photon.

Almost all forces we experience in daily life apart from gravity can be explained by electromagnetism. Classical electromagnetism describes electromagnetic field using Maxwell's equations and the electromagnetic force by the Lorentz force law, which states that $\mathbf{F} = q(\mathbf{E}+\mathbf{v}\times\mathbf{B})$. The four Maxwell's equations are:

- Gauss's law for electricity: $\nabla \cdot \mathbf{E} = \frac{\rho}{\epsilon_0}$
- Gauss's law for magnetism: $\nabla \cdot \mathbf{B} = 0$
- Faraday's law of induction: $\nabla \times \mathbf{E} = -\frac{\partial \mathbf{B}}{\partial t}$
- Ampere's law with Maxwell's correction: $\nabla \times \mathbf{B} = \mu_0 \left(\mathbf{J} + \epsilon_0 \frac{\partial \mathbf{E}}{\partial t}\right)$

These equations are covariant under *Lorentz Transformation*, preserving the speed of light. Thus, Maxwell's equations are relativistic (and incompatible with Galilean relativity).

Quantum electrodynamics (QED) is the relativistic quantum field theory version of classical electrodynamics describing all phenomena involving electric charges in the Standard Model. In QED, the electromagnetic field (denoted by B_μ) is quantized, interaction terms between charged particles and the electromagnetic field are introduced in the Lagrangian, and divergent quantities are renormalized. QED is an abelian gauge theory defined on the *Minkowski space* having the symmetry group $U(1)$ – the circle group, with the electric charge operator Q as the generator.

Historically, the formalization of QED introduced gauge theory and renormalization to describe a fundamental force, motivating the development of *quantum chromodynamics* and *electroweak theory* to describe the other forces.

1.3.2 Strong Force

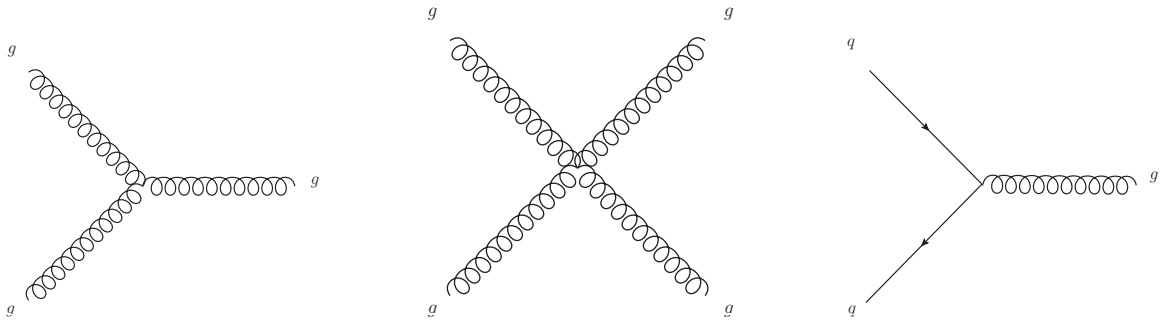

(a) (b) (c)

Figure 1.4: Basic Feynman diagram vertices of the strong interaction

The strong force is a short-range force restricted to subatomic ranges. It holds quarks together to form the hadrons and binds the protons and neutrons together in the nucleus of atoms. Quantum chromodynamics (QCD) is the quantum field theory that describes the strong force between colour-charged particles mediated by gluons. It is a non-abelian gauge theory with symmetry group $SU(3)$ – an 8-dimensional Lie group with all 3×3 unitary matrices having determinant equal to 1 as its elements. Unlike electric charge, there are three colours and three anticolours in quantum chromodynamics. As mentioned in section 1.2.2.2, the eight generators of QCD correspond to the eight gluons. QCD has the following properties:

- Colour confinement: Colour-charged particles cannot be isolated as it is energetically favourable to create additional quark and antiquark pairs from the vacuum to form composite colourless particles.

- Asymptotic freedom: The coupling strength of the strong force decreases at high energies, and hence, the strong interaction becomes asymptotically weaker as the energy scale of the interactions increases.

1.3.3 Weak Force

The weak force description has been unified with the electromagnetic force, and the unified theory is termed electroweak interaction. The electroweak theory (EWT) is a non-abelian gauge theory of $SU(2) \times U(1)$ gauge group. $SU(2)$ is a 3-dimensional Lie group with all 2×2 unitary matrices

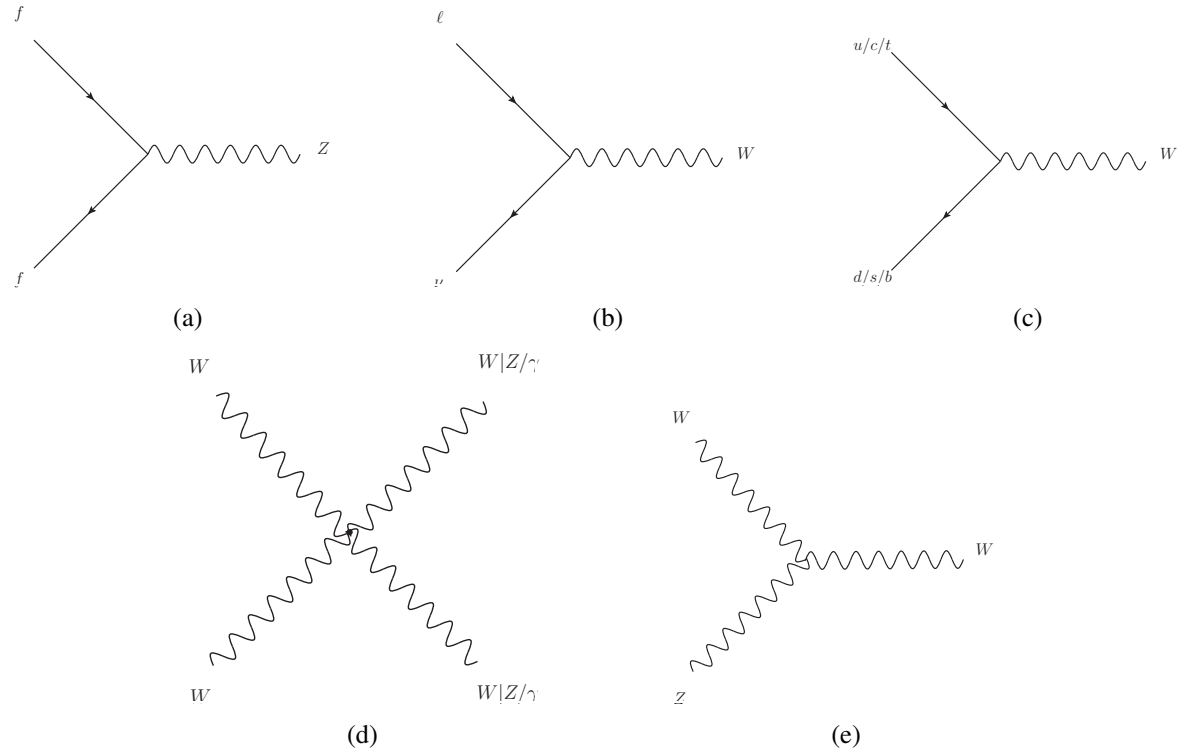

Figure 1.5: Feynman vertices of the Weak interaction. Here f represents any fermion, ℓ represents any charged lepton (i.e., e, μ, or τ) and ν represents a neutrino.

having determinant equal to 1 as their elements, and the corresponding gauge fields are denoted as W^a_μ ($a \in \{1, 2, 3\}$). The weak interaction is mediated by W^+, W^- and Z^0 bosons produced by the spontaneous symmetry breaking of the electroweak symmetry by the Higgs mechanism. All fermions interact with the weak force. Weak interaction is the only interaction that can change the flavour of quarks and leptons, and the only interaction to violate *parity symmetry* and *charge-parity symmetry*.

Weak isospin (T_3) is a quantum number which tells how a particle interacts with $W^\pm$ bosons. In the Standard Model, all the right-handed fermions have weak isospin 0, and all the left-handed fermions have weak isospin $\in \{+\frac{1}{2}, -\frac{1}{2}\}$. Particles with 0 weak isospin (e.g. right-handed fermions) do not interact with the $W^\pm$ bosons. *Weak hypercharge*, defined as $Y_W = 2(Q - T_3)$ is the generator of the electroweak gauge group's $U(1)$ component. Both weak isospin and weak hypercharge remain conserved in all interactions except interactions with the Higgs field.

Similar to weak isospin, the *weak charge* (Q_w) of a particle tells how it interacts with the Z^0 boson.

1.4 Limitations of the Standard Model

Though the Standard Model is the most successful theory, it still can not explain various phenomena—it is an incomplete theory. This has inspired physicists to search for physics beyond the

Standard Model for a more fundamental theory. In this section, we list some of the limitations of the Standard Model.

1.4.1 Gravity

The Standard Model doesn't include gravity in its description. Gravity is described by the geometry of spacetime according to Einstein's general theory of relativity. Gravity arises from the curvature of spacetime caused by the presence of mass or energy. The Standard Model describes the strong, electromagnetic and weak interaction using gauge quantum field theories. These forces are mediated by force-carrying bosons, which have been experimentally observed. The biggest challenge to developing a quantum theory of gravity is that the general theory of relativity is non-renormalizable using standard techniques of quantum field theory. The hypothetical boson corresponding to quantum gravity, the *graviton*, has not been observed experimentally. *String theory*, *loop quantum gravity* and *causal dynamical triangulation* are some approaches to quantum gravity.

1.4.2 Dark matter

It has been hypothesized that there is a kind of matter that does not interact with electromagnetic force and is only affected by gravity. This kind of matter is termed *dark matter*. It makes up approximately 85% of the matter of the universe and around 27% of the mass-energy content.

Some observations that indicate the presence of dark matter are:

- Galaxy rotation curves: It has been observed that the orbital speed of matter remains roughly the same as the distance from the centre of the galaxy increases, which is in contrast to what is expected if the luminous mass was the only matter in the galaxy. The rotation curves suggest that a lot of dark matter is towards the periphery of the galaxies.

- Gravitational lensing: The distortion geometry of clusters or the shear deformation of the background galaxies can be compared to the light ratios, and dark matter distribution can be mapped.

- Galaxy clusters: Masses of galaxy clusters can be measured in three ways: 1) radial velocities of the galaxies in the cluster, 2) X-ray spectrum, flux and radiation pressure, and 3) gravitational lensing. All three methods indicate the presence of dark matter in roughly the same proportion.

- Cosmic microwave background (CMB) anisotropy: Unlike ordinary matter in the early universe, dark matter does not involve in Thomson scattering. Thus, they perturbed the CMB differently, and this can be measured by plotting the angular power spectrum of the CMB.

A few dark matter candidates are: 1) *weakly interacting massive particles* (WIMPs), 2) *massive astrophysical compact halo objects* (MACHOs) like primordial black holes, neutron stars or brown dwarfs, 3) *axions*, and 4) *sterile neutrinos*.

1.4.3 Dark Energy and the Cosmological Constant Problem

Distance measurements with cosmological redshift suggest that the universe's expansion is accelerating. As gravity tends to shrink the universe or decelerate the expansion, to explain the accelerated expansion, a form of energy like *vacuum energy* is required. This unknown form of energy permeating through space is called dark energy, and it can also explain the flat geometry of the universe. A *lambda-CDM* model has been proposed, which estimates dark energy to make up roughly 68% of the total mass energy of the universe. The vacuum energy density calculated using quantum field theory exceeds the observed vacuum energy density by 120 orders of magnitude. This is known as the *cosmological constant problem*.

1.4.4 Hierarchy Problem of Higgs Mass

The weak force is 10^{24} times stronger than gravity. The *Fermi constant* is expected to be near *gravitational constant* unless there is a delicate cancellation by the quantum corrections. This can also be posed as to why the Higgs boson's mass is so less compared to the *Planck mass*. This is an example of a fine-tuning problem in physics.

1.4.5 Neutrino Oscillation

According to the Standard Model, any neutrino created with a specific lepton flavour should have the same flavour in its lifetime. It has been observed in various observations, especially solar neutrino experiments, that neutrino flavour changes as it propagates through space. This is known as *neutrino oscillation*. The Standard Model says that neutrinos are massless. However, to explain neutrino oscillation, neutrinos must possess non-zero mass.

Many BSM (beyond standard model) theories have been proposed to explain how neutrinos might acquire mass. Some of them postulate the existence of right-handed neutrinos (as mentioned in 1.2.1.2, only left-handed neutrinos exist in the Standard Model). We discuss right-handed neutrinos in section 1.5.2 and in chapter 3.

1.5 Beyond the Standard Model

BSM Theories such as Grand Unified Theory (GUT), supersymmetry (SUSY), and Extra-Dimension models were proposed to address the shortcomings in the SM. Usually, such models require the existence of heavy BSM particles. We discuss two such particles relevant to our work – leptoquarks and right-handed neutrinos.

1.5.1 Leptoquarks

Leptoquarks (LQs) are hypothetical particles that can simultaneously couple with quarks and leptons. They are color-triplet scalar (spin 0) and vector (spin 1) bosons that carry both lepton and baryon numbers. They are electromagnetically charged and can exist as a weak singlet, doublet, or triplet. LQs naturally occur in theories such as Pati-Salam models, SU(5) GUTs, Technicolor models. Their connection to the lepton and color sector makes them one of the ideal candidates to explain the anomalies in B-physics.

Up-type quarks have a charge of $+\frac{2}{3}$, and down-type quarks have a charge of $-\frac{1}{3}$. Electrons, muons and taus have a charge of -1 and neutrinos have no charge. Thus, a leptoquark decaying to a quark and a lepton can have the following values of electric charge:

- $Q = +\frac{5}{3}$ (up-type quark and a charged anti-lepton)
- $Q = +\frac{2}{3}$ (up-type quark and a neutrino; down-type quark and a charged anti-lepton)
- $Q = -\frac{1}{3}$ (down-type quark and a neutrino; up-type quark an a charged lepton)
- $Q = -\frac{4}{3}$ (down-type quark and a charged lepton).

As there are three up-type quarks, three down-type quarks, three charged leptons, and three neutrinos, a leptoquark with a given charge can yield $(3 \times 3 =)$ 9 different interaction types. The resulting coupling constants per interaction type can be listed as a 3×3 matrix, as shown in eq. 1.1. Additionally, based on their spin, they can be classified as scalar (spin 0) or vector (spin 1) leptoquarks.

$$\text{Coupling Matrix} \equiv \begin{pmatrix} \lambda_{11} & \lambda_{12} & \lambda_{13} \\ \lambda_{21} & \lambda_{22} & \lambda_{23} \\ \lambda_{31} & \lambda_{32} & \lambda_{33} \end{pmatrix} \tag{1.1}$$

Here, for λ_{ab}, the first index a specifies the quark generation number, and the second index b specifies the lepton generation. We use the Yukawa coupling matrices later in chapter 6 (equation 6.1).

1.5.2 Right-Handed Neutrinos

All fermions in the Standard model, except neutrinos, can have both left-handed chirality and right-handed chirality. As mentioned in section 1.2.1.2, left-handed neutrinos interact only via the weak force as they possess neither the electric charge nor the colour charge.

Neutrino oscillation observations imply that the left-handed neutrinos have some non-zero mass, which is in contrast to the Standard Model's prediction. The simplest explanations propose the existence of right-handed neutrinos to allow the introduction of the Dirac mass term. They are often referred to as *sterile neutrinos* as they are not expected to interact with any SM gauge bosons. They can, however, interact with leptoquarks if they exist (discussed extensively in chapter 3). Right-handed neutrinos can have masses in the range 1 eV to 10^{21} eV. They can also be used to explain other unexplained phenomena in cosmology, like dark matter.

Chapter 2

Essential Concepts: The Experimental Setup and Tools

2.1 Particle Accelerators

The Standard Model lists twelve fermions and five bosons, some of which are short-lived and decay to lighter particles. Energetic collisions happen in the stars, and the byproducts reach our planet as *cosmic rays*. These high-energy cosmic rays which bombard Earth's atmosphere produce particles like muons, pions and neutrinos on their way to the ground. Another alternative to studying fundamental particles is to build our own *particle accelerators*. Particle accelerators accelerate charged particles to very high speeds and collide them at these high energies. This results in the production of short-lived particles which either reach the detectors or give unique signatures. Unlike cosmic rays, particle accelerators can be designed according to our requirements. Other methods to test the Standard Model and search for new physics include 1) Neutrino experiments, 2) Dark matter detectors (and telescopes), etc.

The current largest particle accelerator is the *Large Hadron Collider* (LHC). The LHC is a circular particle accelerator that is 27 kilometres in circumference and located about 175 meters underground. It can collide 1) proton – proton, 2) heavy ion – heavy ion, and 3) proton – heavy ion at energy levels at the TeV scale. For reference, the mass of an electron, one of the lightest particles, has a mass of about 0.5 MeV/c^2, and the mass of a top quark, the heaviest particle in the Standard Model, is around 173 GeV/c^2. The LHC will be upgraded to High Luminosity Large Hadron Collider (HL-LHC) after the current run. Our study (chapter 3) focuses on the discovery prospects at the HL-LHC.

2.1.1 Luminosity

The *instantaneous luminosity* (or just *luminosity*) of a particle accelerator is a measure of the number of collisions that can be produced per unit cross-sectional area and unit time. Mathematically, it is expressed as:

$$L = \frac{f \times N_1 \times N_2}{A} \tag{2.1}$$

where L is the luminosity, N_1 is the number of particles in the first bunch, N_2 is the number of particles in the second bunch, f is the frequency of particle bunches colliding at the detector, and A is the cross-sectional area of the particle bunches. LHC's peak luminosity is of the order 10^{34} cm^{-2}s^{-1}. HL-LHC's peak luminosity will be around 7.5×10^{34}cm^{-2}s^{-1} [2]. The higher the luminosity, the more collisions occur.

The *integrated luminosity* is the integral of the luminosity with respect to time.

$$L_{int} = \int L \, dt \tag{2.2}$$

2.1.2 Beam Energy

The total of the kinetic energy of the colliding particles is known as the *collision energy*. The collision energy for the LHC is around 13.6 TeV and for HL-LHC is around 14 TeV. When particles of the same mass collide, each of them has roughly the same kinetic energy in the detector frame, i.e., half of the collision energy. The kinetic energy of a single particle is known as *beam energy* of the respective beam.

Higher energy collisions increase the probability of the production of high-mass particles.

2.1.3 Parton Distribution Function

Baryons have three quarks, and mesons have a quark and an antiquark. These quarks are known as *valence quarks*. Apart from the valence quarks, hadrons have quarks and gluon fields that constantly create and destroy quarks and gluons. The virtual quarks are called *sea quarks*. Thus, a hadron is composed of many point-like constituents called *partons*.

The (longitudinal) momentum fraction of partons within a hadron is defined by the *parton distribution function* (PDF). PDF $f_q(x, Q^2)$ represents the probability density to find a parton q carrying a momentum fraction x.

2.1.4 Cross-section

Cross-section of a process measures the probability of an interaction to occur if two particles come close to each other, like in a particle collider. In classical physics, the cross-section of two colliding particles is the area transverse to their relative motion within which they must meet to scatter. In quantum scattering, the cross-section can be better thought of as a 'scattering probability' parameter.

The cross-section, σ, can be related to the number of events that occur, $\mathcal{N}$, and the luminosity, L, as

$$\mathcal{N} = L \, \sigma \tag{2.3}$$

2.1.5 Efficiency

Once an interaction takes place at the collider, the particles often decay into other products on their way to the detector and leave a signature. This detection has to be interpreted correctly if we count the number of events of interest that take place, and there remains a fraction of events that occurred which are not successfully detected. We define detector efficiency ϵ_{det} as the fraction of events successfully detected.

In the following sections, we describe how we search for particular signals amid background processes that give similar particles as decay products. To eliminate background processes, we look at various parameters of the detection and eliminate events that have parameter values not expected from signal events. Therefore, the outlier signal events and background events outside the parameter threshold (cut) region are rejected, decreasing the number of events considered. This is known as cut efficiency ϵ_{cut}. Thus,

$$\mathcal{N} = \sigma \times \epsilon \times L \tag{2.4}$$

where ϵ is the overall efficiency,

$$\epsilon = \epsilon_{det} \times \epsilon_{cut} \tag{2.5}$$

2.1.6 Branching Fraction

Often, a particle can have multiple decay modes where the decay products vary. Some decay modes are more likely than others. The *branching fraction* is the probability that a particular decay mode will occur if a particle decays. It is usually represented by β or $\mathcal{B}$.

Example: We know W^+ bosons can decay either leptonically or hadronically. The branching fractions for them are $\frac{1}{3}$ and $\frac{2}{3}$, respectively. For the leptonic decays, $\mathcal{B}(e^+\nu_e) = \mathcal{B}(\mu^+\nu_\mu) = \mathcal{B}(\tau^+\nu_\tau) = \frac{1}{9}$.

2.2 Lagrangian

The *Principle of Least action* states that the solutions of equations of motion of a system are the *stationary points* of the system's *action functional*. Action is a function that gives a real number for every trajectory of the system. Mathematically, action ($\mathcal{S}$) is described as:

$$\mathcal{S} = \int \mathcal{L}\, d^4x \tag{2.6}$$

where $\mathcal{L}$ is the *Lagrangian density* of the system. It is a function of quantum fields and their derivatives, encoding the kinetic and potential energies of the field. The interactions in the Standard Model and BSMs are described by Lagrangians. We briefly describe the lagrangian we use later in section 3.1.

$$\mathcal{L} \supset \ \lambda_1 \bar{s}_L \nu_R \phi_1 + \lambda_2 \bar{c}_L \nu_R \phi_2 + \text{H.c.} \tag{2.7}$$

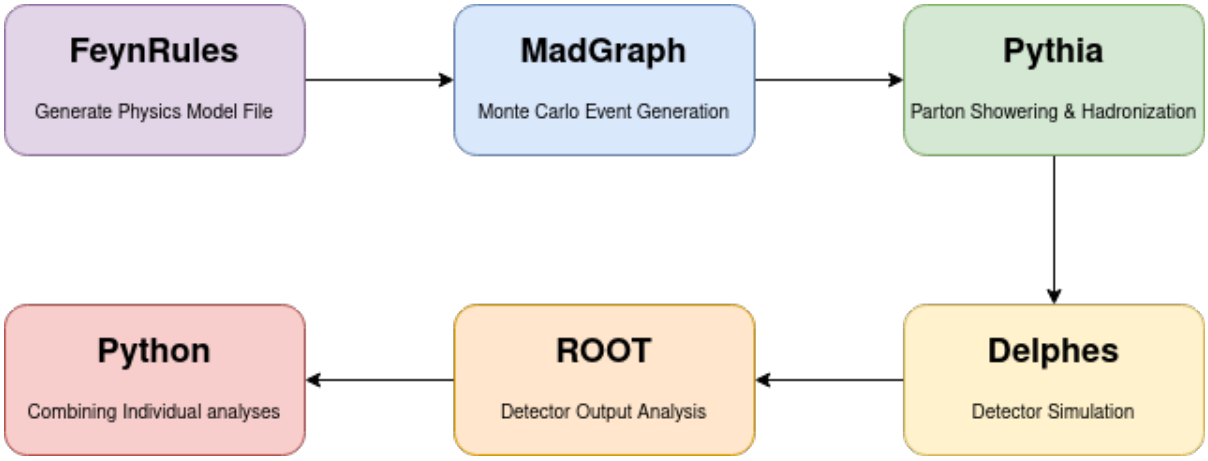

Figure 2.1: Software packages and the analysis chain.

Here, ϕ_1 and ϕ_2 denote scalar leptoquark fields with EM charge $1/3$ and $2/3$ respectively. $\bar{s}_L$ and $\bar{c}_L$ denote strange and charm spinor fields, ν_R denotes RHN spinor field. λ_1 and λ_2 denote the $\phi\ell q$ coupling terms.

2.3 Software Packages

An experiment at a particle collider can be roughly divided into four stages:

1. proton-proton (or any particle-particle) collision, which results in the formation of new products.
2. decay of the short-lived products on their way to the detector. This also includes *parton showering*.
3. detection of products or their subsequent decay products at the detector.
4. analysis of the data from the detector by physicists.

Physicists often need to predict the results of experiments using computers. Given the complex interactions involved, it is very difficult to compute these results analytically. Rather, Monte Carlo simulations with appropriate probability distributions are done to simulate the particle collider. Specialised software packages have been developed for each stage. We discuss the packages that we have utilised for our work below. Fig. 2.1 briefly shows the packages and their utilities.

2.3.1 FeynRules

Before any particle-particle collision is simulated in a computer, the underlying physics has to be specified and formulated programmatically. FeynRules is a package that takes particle physics models formulated using a list of fields, parameters, and Lagrangians and calculates the underlying Feynman

rules. It can then output these rules as a UNIVERSAL FEYNRULES OUTPUT (UFO) file, which various Monte Carlo event generator packages can use.

2.3.2 MADGRAPH

MADGRAPH takes the UFO files as the physics model and does Monte Carlo event generation of the desired processes. Internally, it computes matrices that contain the probability amplitudes for how a given set of initial states of incoming particles can produce a final state of outgoing particles. This involves computing the Feynman diagrams for the interaction. The event sample generated at the end of the Monte Carlo simulation can be used for further analysis. Cross-sections, branching fractions, etc., of any process can also be computed.

2.3.3 PYTHIA

The outgoing particles can contain gluons and quarks, which further decay, giving a cascade of secondary, less energetic particles. This is termed as *parton showering*. It is difficult to compute matrix elements for higher-order QCD interactions as the subsequent fragmentation of these particles is non-perturbative and involves many low-energy particles. Pythia is a Shower Monte Carlo program which simulates parton showering by randomly sampling shower parameters like splitting angles. It can also do Monte Carlo event generation.

Due to color confinement, colored particles like quarks and gluons cannot freely exist and, thus, combine to form color-neutral hadrons like protons and neutrons, i.e., they hadronize. Pythia is also used to hadronize its generated parton shower.

2.3.4 DELPHES

The response of the detector is simulated in DELPHES. It takes the output from MADGRAPH or PYTHIA and applies detector simulation algorithms to simulate the detector's response to the generated events. It takes care of multiple scattering, detector resolution and energy losses. It can simulate various detectors like CMS and ATLAS by taking the detector specifications as inputs.

2.3.5 ROOT

ROOT is used to analyse simulation data in particle physics. Simulation data or any C++ object can be stored as a compressed binary in a ROOT (*.root) file. The data is stored in a tree data structure which enables fast access to huge data which can be spread over multiple places. It also provides functionalities to model data, do parallel processing, and produce plots. It provides a C++ interpreter and allows ROOT code to be written in other languages (like PYTHON) using bindings.

Using C++ with ROOT, we can analyze the detector simulation data we receive from DELPHES. The same code can be used to study the actual experimental data from particle accelerators.

Chapter 3

Right-Handed Neutrinos through Leptoquarks at the Large Hadron Collider

We discussed neutrino oscillation as evidence of the presence of physics beyond the Standard Model in section 1.4.5. Neutrino oscillation suggests that the neutrinos of the Standard Model (i.e., left-handed neutrinos) have mass. Neutrinos are very light and pass through most material without interacting, and thus, are difficult to detect at particle accelerators. One possible explanation for neutrino mass is the existence of their heavier counterparts called right-handed neutrinos (RHNs, ν_R's). These RHNs, if they exist, could be produced in particle colliders like the Large Hadron Collider (LHC) and could help us understand the origin of neutrino mass and other important questions in physics, like dark matter and matter-antimatter asymmetry.

The common explanations of RHNs predict that these particles would be too heavy to produce at the LHC. There are alternative explanations (like the *inverse seesaw mechanism*) which predict RHN mass to be within the limits of LHC. However, even these lighter RHNs are difficult to detect because they interact feebly with SM particles [3]. We consider RHN production through leptoquarks (LQ) as LQs are predicted to have high masses and can be formed in hadron colliders like LHC.

LQs (discussed in section 1.5.1) are hypothetical coloured scalar or vector bosons with both baryon and lepton numbers. They appear in various BSM theories and are often used to explain experimental anomalies. The phenomenology of LQs and their discovery prospects at different colliders can be found in Refs. [4–13].

The LHC is investigating the single and pair productions of LQs in various combinations of charged leptons, neutrinos and jets in the final state. In this context, the current mass-exclusion limits on scalar LQs go up to 1.73 [14] TeV. Indirect bounds on LQ couplings (LQ-quark-lepton) from the high-p_T dilepton or monolepton with missing energy data are available in [15, 16]. However, none of the direct or indirect bounds concerns LQ's coupling with a SM quark and a RHN. If a LQ predominantly decays to a RHN and a quark, the parameter space becomes unrestricted by all the direct and indirect bounds.

We try to bridge the gap by studying the production of RHNs via LQs (like in Refs. [17–21]) assuming that they couple with no leptons other than RHNs. Thus, RHNs can be produced either by LQ

decays or by t-channel LQ exchange, as shown in fig 3.1. We also note that the t-channel processes involve the fourth power of λ, the LQ-quark-lepton coupling.

For the LHC to detect their signatures, the RHNs should not be long-lived and decay to SM particles within the detectors. In the models we consider, RHNs decay mainly through the $\nu_R \to W^{\pm}\ell^{\mp}$ and $\nu_R \to Z/h\ \nu_\ell$ processes in roughly $2:1:1$ ratio. As discussed in section 1.5.1 and in eq 1.1, LQs can have inter or intra-generational couplings (i.e., the quark and the lepton that couple to a LQ need not be of the same generation). We consider second-generation interactions where the LQ decays to a second-generation quark (strange or charm) and a second-generation RHN (λ_{22}) mainly because the muon detection efficiency is better than the electron detection efficiency at the LHC.

3.1 A Simple Model

From the LQs mentioned in [22], we consider the sLQs that can exclusively decay to second-generation quarks and right-handed neutrinos. Similar to [9, 11, 23], we can write a simplified phenomenological Lagrangian as,

$$\mathcal{L} \supset \lambda_1 \bar{s}_L \nu_R \phi_1 + \lambda_2 \bar{c}_L \nu_R \phi_2 + \text{H.c.}, \tag{3.1}$$

where s and c represent strange quark and charm quark, respectively. ϕ_n denotes a charge-$n/3$ scalar LQ. We model the interactions of ϕ_1 and ϕ_2 by considering only one λ.

3.2 LHC Phenomenology

We implement the phenomenological Lagrangian terms in FEYNRULES [24] to generate UNIVERSAL FEYNRULES OUTPUT (UFO) files [25] needed for MADGRAPH5 [26] to generate the signal and background events at the leading order. Whenever available, we account for higher-order cross-sections with appropriate K factors. In particular, among the signal processes, we use a typical K-factor of 1.5 for the pair production of the scalar LQs [27–29]. We pass the parton-level events first through PYTHIA8 [30] for showering and hadronization and then through DELPHES3 [31] for detector simulation with the default CMS card. The jets are reconstructed from the DELPHES tower objects with anti-k_T clustering algorithm [32] in FASTJET [33]. We use jets of two different radii in our analysis: (a) AK4 jets with $R = 0.4$ and (b) AK8 fatjets with $R = 0.8$.

3.2.1 Production at the LHC

In fig 3.1, we show a few of the production processes that can give two RHNs. Fig 3.1a shows LQ resonant pair production. The monoleptonic decay of this process is shown in fig 3.3. Fig 3.1b shows the single production of a LQ and a ν_R, mediated by the LQ-quark-RHN coupling, λ. Fig 3.1c shows the single production of LQ with a quark and ν_R. In fig 3.1d, a LQ appears in the t-channel

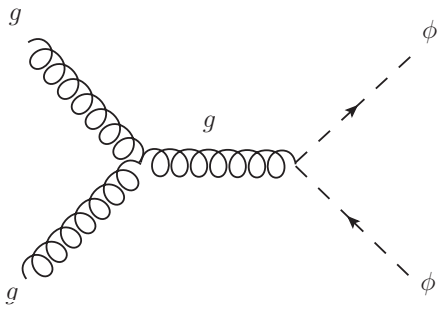

(a) Pair Production: $q\,q \to \phi\,\phi$

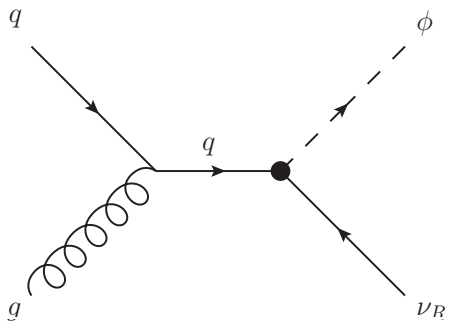

(b) Single Production – s-channel: $p\,p \to \phi\,\nu_R$

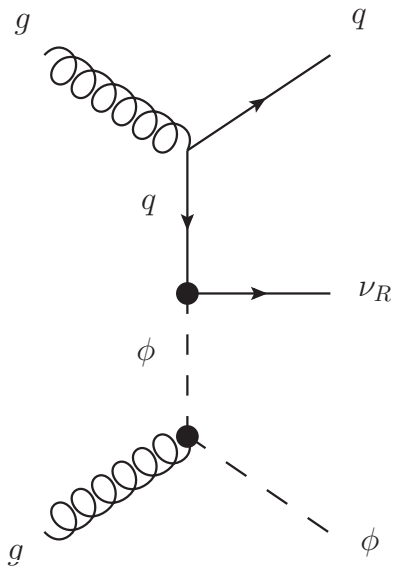

(c) Single Production: $p\,p \to \phi\,\nu_R\,j$

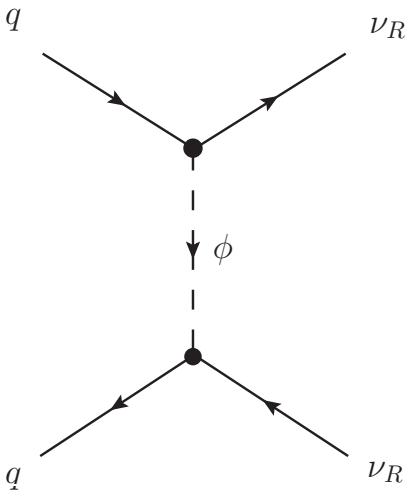

(d) T-channel: $p\,p \to \nu_R\,\nu_R$

Figure 3.1: Leptoquark and right-handed neutrino production modes. The leptoquark ϕ further decays to a quark q and a right-handed neutrino ν_R.

and contributes to the RHN pair production, $qq \to \nu_R\nu_R$. In fig 3.2, we show the cross-sections for the production processes for $M_{\nu_R} = 500$ GeV and $\lambda = 1$. Note that while t-channel cross-sections are smaller than the pair and single LQ production cross-sections for lower LQ masses, the t-channel process becomes important for large couplings as its cross-section grows as λ^4.

Since there is no direct experimental bound on the LQs decaying exclusively through RHNs, they can be even lighter than a TeV. However, we mainly focus on the $M_{\rm LQ} \geq 1$ TeV and $M_{\nu_R} \sim 500$ GeV region of the parameter space. In our computations, we include the contributions of all the above ν_R-production processes to estimate the signal significance.

The RHN pair production processes can be classified in terms of the number of charged leptons in the final state. In principle, it is possible to get three or more muons in the final state, where the extra leptons come from the decays of the vector bosons. However, since the leptonic branchings of the heavy

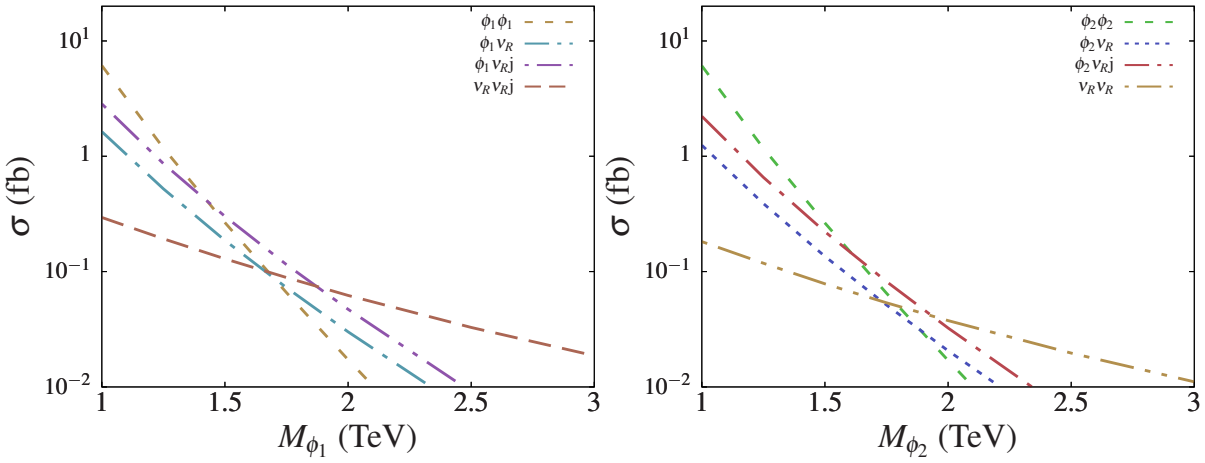

(a) (b)

Figure 3.2: Cross-sections of production modes of ϕ_1 (a) and ϕ_2 (b). We also show the cross-section of RHN pair production through t-channel LQ exchange. The LQ single productions and RHN pair production process are computed for $\lambda = 1$.

vector bosons are smaller than their hadronic branchings, we do not consider final states with more than two muons.

(a) **Monolepton final state**: Ones with a muon accompanied by jet(s), fatjet(s) (from the hadronic decays of heavy bosons generated in the ν_R decay) and some missing E_T. The different production modes contribute in the following manner:

$$pp \to \left\{ \begin{array}{l} \phi\phi \\ \phi\,\nu_R \\ \nu_R\nu_R \end{array} \right\} + \text{jet(s)} \to \left\{ \begin{array}{l} (j\nu_R)(j\nu_R) \\ (j\nu_R)\nu_R \\ \nu_R\nu_R \end{array} \right\} + \text{jet(s)} \to \mu^{\pm} W_h^{\mp} Z_h \nu_L + \text{jet(s)}.$$

(b) **Dilepton final state:** Ones with a opposite-sign muon pair ($\mu^+\mu^-$) plus jet(s) and fatjet(s). The different processes contribute to the dilepton final states as

$$pp \to \left\{ \begin{array}{l} \phi\phi \\ \phi\,\nu_R \\ \nu_R\nu_R \end{array} \right\} + \text{jet(s)} \to \left\{ \begin{array}{l} (j\nu_R)(j\nu_R) \\ (j\nu_R)\nu_R \\ \nu_R\nu_R \end{array} \right\} + \text{jet(s)} \to \mu^{\pm}\mu^{\mp} W_h^{\pm} W_h^{\mp} + \text{jet(s)}.$$

The subscripts h and μ denote the hadronic and leptonic decays of vector bosons, respectively. A dimuon final state can also come from $\nu_L\nu_L Z_h Z_\mu$ + jet(s) final states. We revisit the monolepton final state in more detail in the following chapter, discuss the reasons for it being more challenging than the dilepton final state, and focus primarily on monolepton final state prospects in this thesis.

We follow a strategy of combining the contributions of multiple signal processes, which follows from refs. [34, 35] where it is shown how one can systematically combine pair and single production events

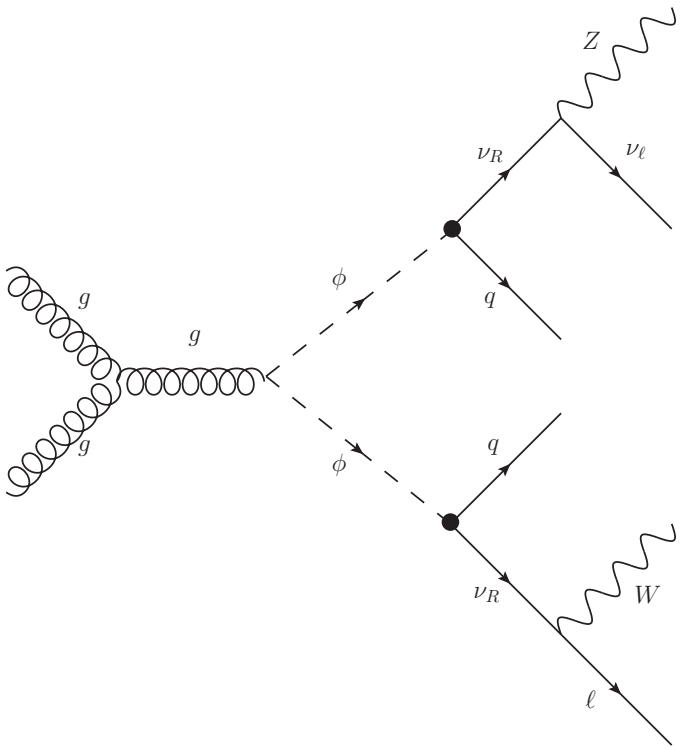

Figure 3.3: $pp \to Z\nu_L W\ell +$ jets. Monoleptonic decay of the pair production mode in figure 3.1a.

leading to the same final states without double counting. Later, in Refs. [9, 11, 23, 36], further use of it is demonstrated. Here, we extend this strategy to the pair production of RHNs.

We extensively discuss event selection strategies to maximize our reach in the next chapter.

Chapter 4

Optimizing Cuts

While searching for the desired event at a particle collider, many background processes with similar decay products also occur. Careful analysis is required to separate the signal and the background processes that mimic the signal. A particle collider like the LHC can capture various properties of particles while detecting them, like the charge, energy and momentum of the particle. Particles corresponding to a particle event can be tracked, and the missing energy (as neutrinos escape the detector without any interaction) can be estimated. By comparing all the properties available to us, we can remove a significant amount of background events.

To find the selection criteria, we can simulate both background and signal events and plot the distributions of various properties available at the detector. Events can be eliminated if they fall above or below a certain threshold where the signal is unlikely to be. We discuss in this chapter how these cuts, i.e., the threshold values, can be estimated. Ideally, a cut should not eliminate more than a few signal events and eliminate most of the background events. This is hard in practice. The strategy is to apply conservative cuts of multiple properties, sequentially reducing the background events while almost all the signal events survive the cut. Also, new properties (like N-subjettiness) can be defined by combining the available properties.

4.1 Signal

In section 3.2.1, we showed the decay products with monolepton and dilepton final states. The dilepton final products are $\mu^{\pm}\mu^{\mp}\, W_h^{\pm} W_h^{\mp}$ + jet(s) (or $\nu_L \nu_L Z_h Z_\mu$ + jet(s)). A significant selection criteria for dilepton final states is that a pair of opposite-sign muons should be detected. This cut eliminates a lot of background. The Monolepton final state is $\mu^{\pm}\, W_h^{\mp}\, Z_h \nu_L$ + jet(s). Unlike the dilepton final state, we do not have any significant property that can single-handedly eliminate a large number of background events. This necessitates us to consider as many independent cuts as possible.

The monolepton signal process is as follows:

$$pp \rightarrow \left\{ \begin{array}{l} \phi\phi \\ \phi\,\nu_R \\ \nu_R\nu_R \end{array} \right\} + \text{jet(s)} \rightarrow \left\{ \begin{array}{l} (j\nu_R)(j\nu_R) \\ (j\nu_R)\nu_R \\ \nu_R\nu_R \end{array} \right\} + \text{jet(s)} \rightarrow \mu^{\pm} W_h^{\mp} Z_h \nu_L + \text{jet(s)} \rightarrow \mu\,\nu_L + \text{jet(s)}$$

For our analysis, we combine the contributions of multiple signal processes. This strategy follows from refs. [9, 11, 23, 34–36] that demonstrated how the experimental reach enhanced by systematically combining pair and single production contributions. As a starting point, we define our inclusive signal selection criteria for the monolepton events as:

A monolepton event must have

- exactly one high-p_T muon and
- at least one high-p_T jet and at least one fatjet from the boosted boson(s).

4.2 Background processes

The background processes which mimic the monolepton signal are:

$$pp \rightarrow W_\ell\,(+2j) \rightarrow \mu\,\overline{\nu_\mu} + 2j \tag{4.1}$$
$$pp \rightarrow W_\ell Z_h\,(+2j) \rightarrow \mu\,\overline{\nu_\mu} + 4j \tag{4.2}$$
$$pp \rightarrow Z_\ell(+2j) \rightarrow \mu^+\mu^- + 2j \tag{4.3}$$
$$pp \rightarrow W_\ell W_h(+2j) \rightarrow \mu\,\overline{\nu_\mu} + 4j \tag{4.4}$$
$$pp \rightarrow t_h W_\ell + t_\ell W_h \rightarrow b\,\mu\,\overline{\nu_\mu} + 2j \tag{4.5}$$
$$pp \rightarrow t_\ell + b/j \rightarrow b\,\mu\,\overline{\nu_\mu} + b/j \tag{4.6}$$

We see that all the background processes have at least one muon and a few jets in the final state. Additionally, in some processes, we get b jet and a neutrino ν_μ. The cross-sections of the background processes are listed in Table 4.1. While generating the processes with very high cross-sections, we apply some basic generational-level cuts to save computation time. Further, we apply selection cuts on these generated events to enhance the signal over background ratio.

4.3 Individual Cuts

In this section, we discuss the parameters necessary to separate signal and background processes. We specify the selection criteria corresponding to each parameter. We also justify the criteria by showing the distribution of the value of parameters for signal and background events. For simplicity, we take the mass of LQ (M_{ϕ_1}) to be 1250 GeV/c^2 and the mass of RHN (ν_R) as 500 GeV/c^2 while plotting the distribution of the parameters in the following figures.

Table 4.1: Cross-sections of the major background processes without any cut [37]. The higher-order cross-sections are taken from the literature; the corresponding QCD orders are shown in the last column. We use these cross-sections to compute the K factors to incorporate the higher-order effects.

Background processes		σ (pb)	QCD order
$V+$ jets [38, 39]	$Z+$ jets	6.33×10^4	N^{2}LO
	$W+$ jets	1.95×10^5	NLO
$VV+$ jets [40]	$WW+$ jets	124.31	NLO
	$WZ+$ jets	51.82	NLO
	$ZZ+$ jets	17.72	NLO
Single t [41]	tW	83.10	N^{2}LO
	tb	248.00	N^{2}LO
	tj	12.35	N^{2}LO

4.3.1 b-tagged Jets

A top quark (t) decays to a W boson and a bottom quark (b). A few of our background processes (4.5, 4.6) involve the top quark and hence, produce b-jets. Our signal, on the other hand, does not involve t and b. DELPHES output contains b-tagged jets. This can be used to separate background processes from the signal by eliminating events which have a b-tagged jet. The following table shows what percentage of events per process contains a b-tagged jet.

Process	% of events with a b-tagged jet
$\phi\phi$ (Pair Production)	34%
$\phi\nu_R$ (Single Production)	30%
W_ℓ	10%
$W_\ell Z_h$	16%
Z_ℓ	9%
$W_\ell W_h$	17%
$t_h W_\ell + t_\ell W_h$	78%
$t_\ell + b/j$	76%

4.3.2 $\not{E}_T$

We have discussed that the left-handed neutrinos interact very faintly with the Standard Model particles and are, thus, difficult to detect. The detectors at the LHC are not capable of detecting neutrinos, and the neutrinos escape with some energy and momentum. By observing the unaccounted energy and momentum of the event, the properties of neutrino can be estimated, assuming that no other stable and sterile BSM particle exists. As the left-handed neutrinos are produced from heavier (500 GeV/c^2) RHNs, the neutrinos from our signal are expected to be boosted, resulting in higher values of $\not{E}_T$, i.e. missing transverse energy.

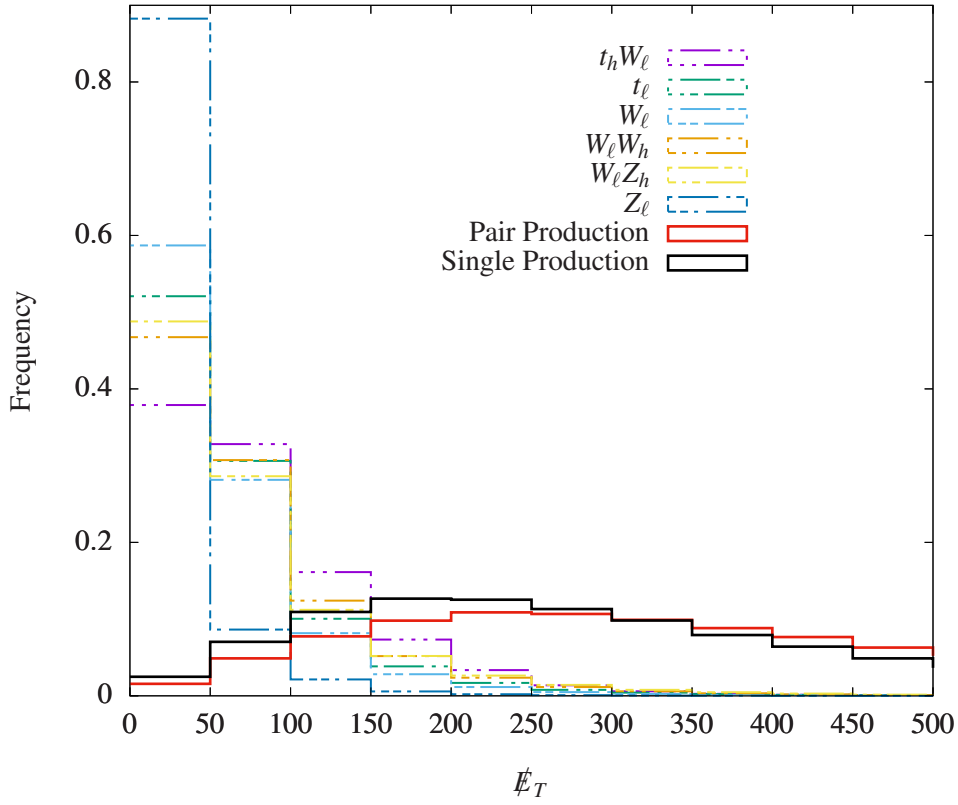

Figure 4.1: Missing Transverse Energy (GeV) per event. $M_{\phi_1} = 1250$ and $M_{\nu_R} = 500$.

In fig. 4.1, we plot the frequency distribution of $\not{E}_T$ for the background processes and signal processes. Indeed, the lower energy bins are populated mostly by background processes, especially in 4.3, where no neutrino is produced, resulting in zero $\not{E}_T$. $\not{E}_t$ for signal events is distributed in higher energy bins. Using this and the grid search method explained later, we set our $\not{E}_T$ cut as:

$$\not{E}_T > 150 \text{ GeV} \tag{4.7}$$

4.3.3 S_T

Due to the conservation of energy, when a heavy particle decays to lighter particles, it imparts them momentum, which is also conserved before and after the decay. The relation can be written as $E_i = E_{f1} + E_{f2}$, where $E^2 = p^2 + m^2$. Thus, if the mass of the decay product remains the same, but the mass of the initial particle is increased, greater momentum is imparted to the decay products to obey the conservation of energy law.

At the LHC, lighter daughter particles can be easily produced than heavier daughter particles due to the underlying parton distribution function (PDF, section 2.1.3). Thus, the average jets originating from lighter daughter particles will have low momenta. In the case of heavier daughter particles, the jets will

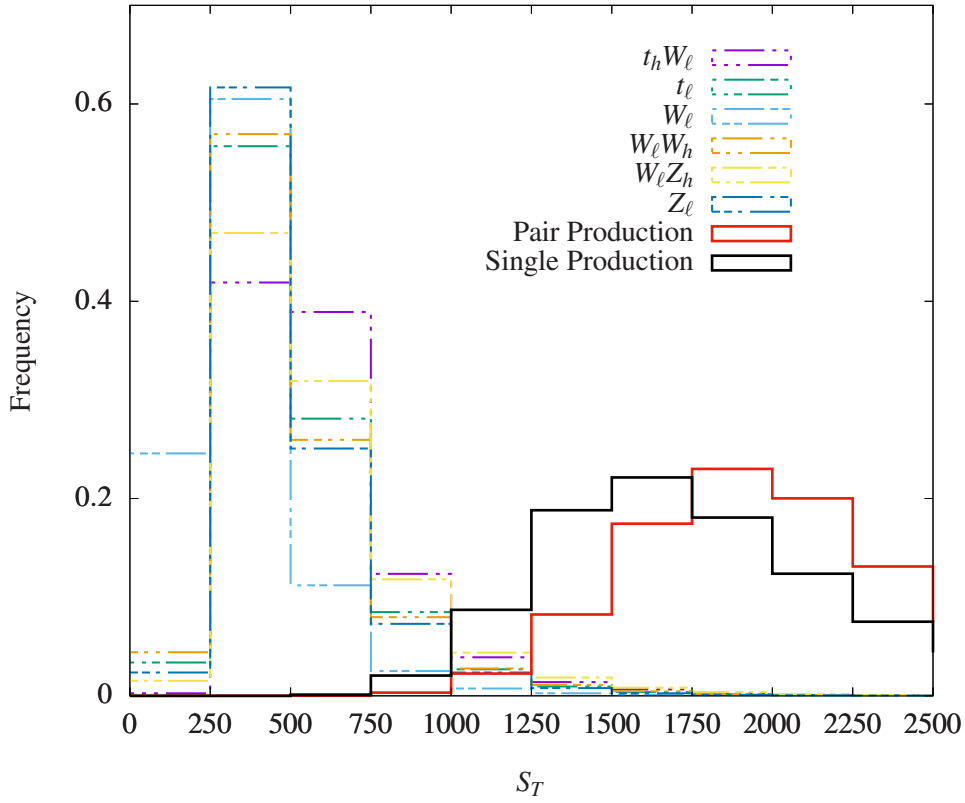

Figure 4.2: Scalar sum of transverse momenta (in GeV/c) of all detected particles per event. $M_{\phi_1} = 1250$ GeV/c^2 and $M_{\nu_R} = 500$ GeV/c^2.

have higher momenta. These jets are referred to as *boosted jets*. Note that we only consider the final *transverse momentum*, p_T, of the products as the initial transverse momentum is zero in the collider. The initial *longitudinal momentum*, on the other hand, is unknown.

In fig. 4.2, we plot the distribution of the scalar sum of the transverse momenta of all jets per event, S_T. The signal events do have much higher S_T than the background processes. The S_T cut is thus,

$$S_T > 1200 \text{ GeV}/c \tag{4.8}$$

4.3.4 $\text{fj}_{\text{H}_\text{T}}$

As discussed earlier, coloured particles undergo hadronization as soon as they are produced, which results in a collimated spray of particles having the same centre-of-mass momentum as the initial coloured particle. These conical spray of particles are called jets. Heavier particles produce jets with larger radii, known as *fatjets*.

Similar to S_T, the fatjets will have higher momenta if they decay from heavier particles. We only consider the transverse component of the momentum for the reason explained in sec 4.3.3. We plot the distribution of the scalar sum of transverse momenta over all fatjets in an event in fig. 4.3.

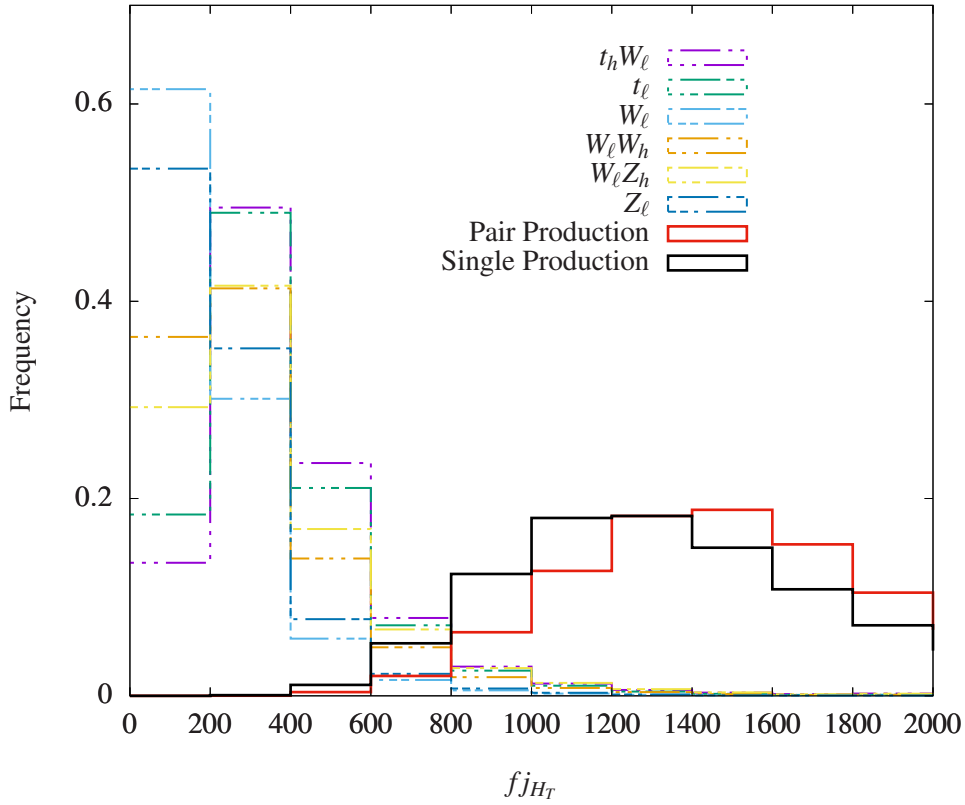

Figure 4.3: Scalar sum of transverse momenta of fatjets (in GeV/c). $M_{\phi_1} = 1250$ GeV/c^2 and $M_{\nu_R} = 500$ GeV/c^2.

This distribution is very similar to fig. 4.2 as both only differ in the number of input jets used to sum the momenta. This correlation, however, implies that the sequential application of these two cuts won't reduce the background as drastically as they would if the criteria were independent.

The $\mathrm{fj_{H_T}}$ cut is then set to:

$$\mathrm{fj_{H_T}} > 600\ \mathrm{GeV/c} \tag{4.9}$$

4.3.5 N-subjettiness

N-subjettiness was introduced in [42]. N-subjettiness indicates the jet shape and how well it can be decomposed to subjets. It is the ratio of the total momentum inside a subregion of the jet to the total momentum of the jet. Jets with N-subjettiness (τ_N) ≈ 0 have N or fewer subjets, whereas jets with $\tau_N \gg 0$ have at least $N + 1$ subjets.

The ratio τ_N/τ_{N-1} is the discriminating variable for N-pronged jet. We utilize this in the following section.

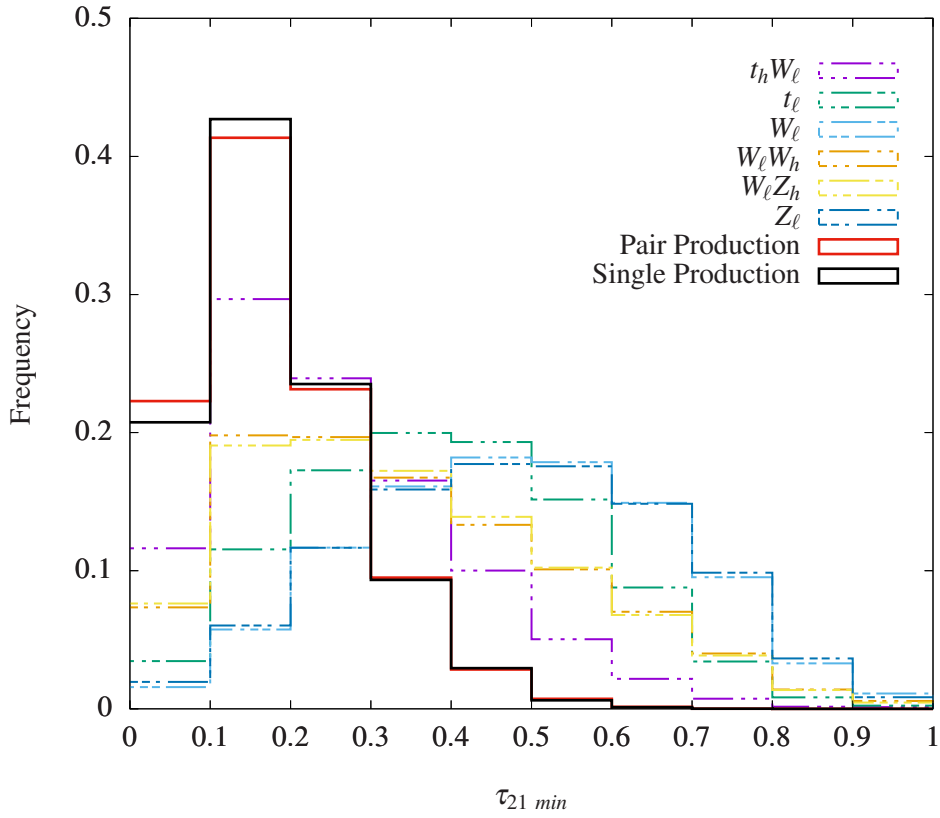

Figure 4.4: Minimum τ_{21}, i.e., N-subjettiness ratio (τ_2/τ_1) among all the fatjets per event.

4.3.5.1 τ_{21}

In our monolepton final state (in sec. 3.2.1), we see that our signal contains one W boson. W decays hadronically into two quarks and, thus, produces a two-pronged jet. The ratio τ_2/τ_1, or simply, τ_{21} can be investigated to search for a W boson. The distribution is shown in fig. 4.4.

As expected, the signal events have lower values of τ_{21}, indicating two prongs. We set the τ_{21} cut to:

$$\tau_{21} < 0.3 \tag{4.10}$$

4.3.5.2 τ_{32}

Few of our background signals contain a top quark, and it can be worthwhile to investigate if this can be used to eliminate some background events. As the top quark decays to a b jet and W boson, this results in a three-pronged jet – one from b jet and two from W boson. Thus, we plot the distribution of τ_{32} in fig. 4.5.

While the distributions of signal and background are slightly different, we do not utilize this cut as the separation is not significant enough. Applying this cut leads to eliminating significant signal

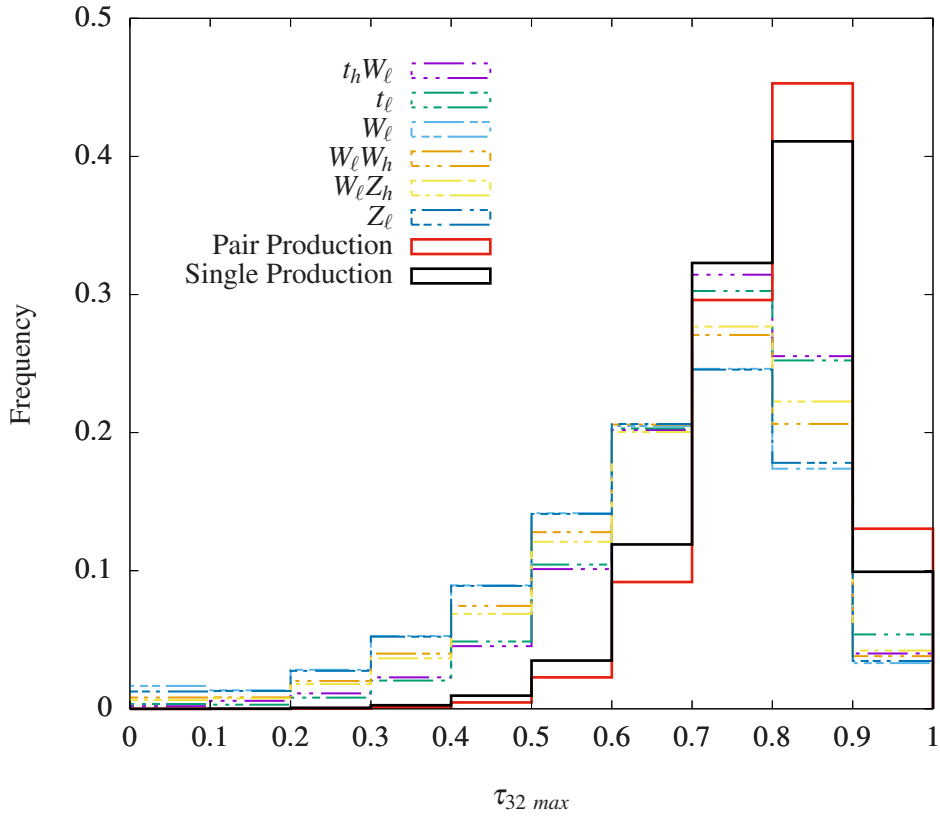

Figure 4.5: Maximum τ_{32}, i.e., N-subjettiness ratio (τ_3/τ_2) among all the fatjets per event.

events, which we do not desire. To eliminate the top quark background, we instead eliminate events with b-tagged jets.

In our code, we set this cut as:

$$\tau_{32} > 0 \tag{4.11}$$

which indirectly means that the cut is not being considered or that all events are allowed to pass this cut.

4.3.6 $M(\text{fj})$

We search for heavier fatjets as the jets originating from W boson would be heavier than average jets. Also, the top quark jets can have higher masses than W jets; thus, we need to restrict those. We plot the distribution of the mass of the heaviest fatjet in each event in fig. 4.6.

The distribution suggests that the first two or three bins be eliminated to eliminate the background. To find the upper limit, we manually test for various values of mass and check how many signals and background processes get eliminated. The optimized cut of $M(\text{fj})$ using the above plot and further analysis is:

$$65 < M(\text{fj}) < 100 \tag{4.12}$$

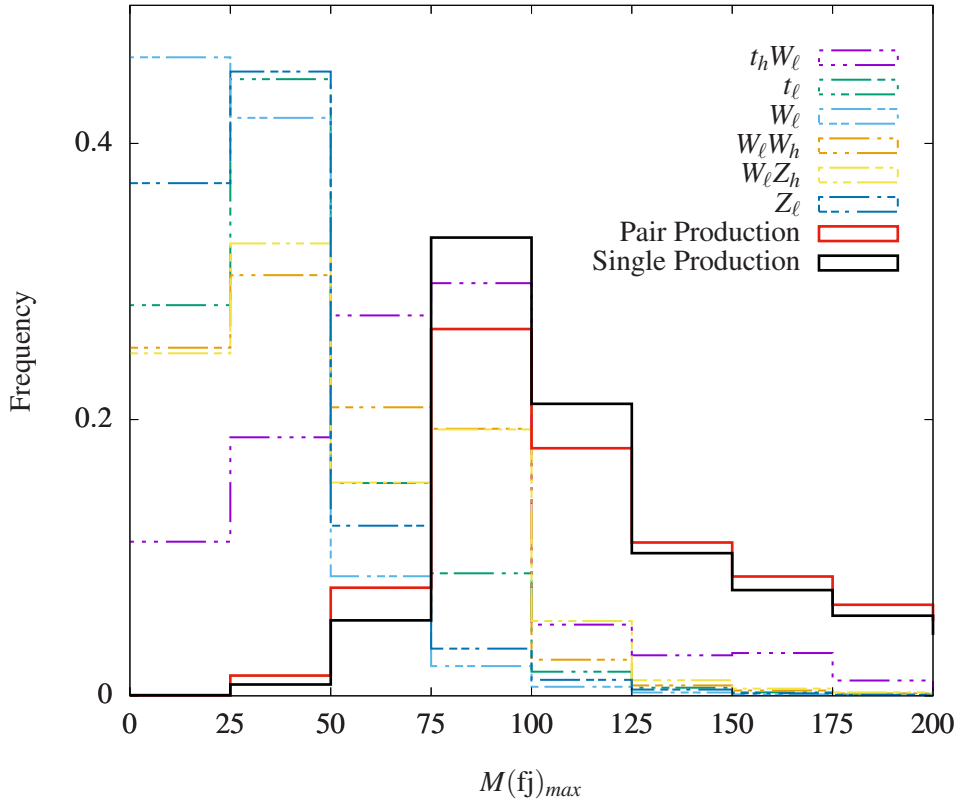

Figure 4.6: Mass of heaviest fatjet per event. $M_{\phi_1} = 1250$ GeV/c^2 and $M_{\nu_R} = 500$ GeV/c^2.

4.3.7 $\Delta R(\text{fj}, \mu)$

$\Delta R(\text{fj}, \mu)$ represents the maximum separation of a fatjet with the muon with the heaviest momentum. Fig. 4.7 shows the distribution of $\Delta R(\text{fj}, \mu)_{\text{max}}$. It seems that the distribution is almost the same for all backgrounds and the signal. Thus, we only apply the following nominal $\Delta R(\text{fj}, \mu)$ cut:

$$\Delta R(\text{fj}, \mu) > 1 \tag{4.13}$$

4.3.8 $p_T(\mu)$

We discussed in section 4.3.3 that 1) heavier daughter particles are less frequently produced than lighter daughter particles, and 2) when produced, the heavier daughter particles have higher average energies than lighter daughter particles. This implies that the decay of heavier daughter particles to products have higher momenta (boost) than the decay products from lighter particles. In our signal, we get a muon (μ) from the decay of a RHN (ν_R) of mass 500 GeV/c^2. Thus, we expect this μ to be boosted, i.e., have a very high momentum.

We plot the distribution of the maximum transverse momentum among muons in Fig. 4.8. The background processes mostly populate the lower momenta bins, whereas the signal processes are well

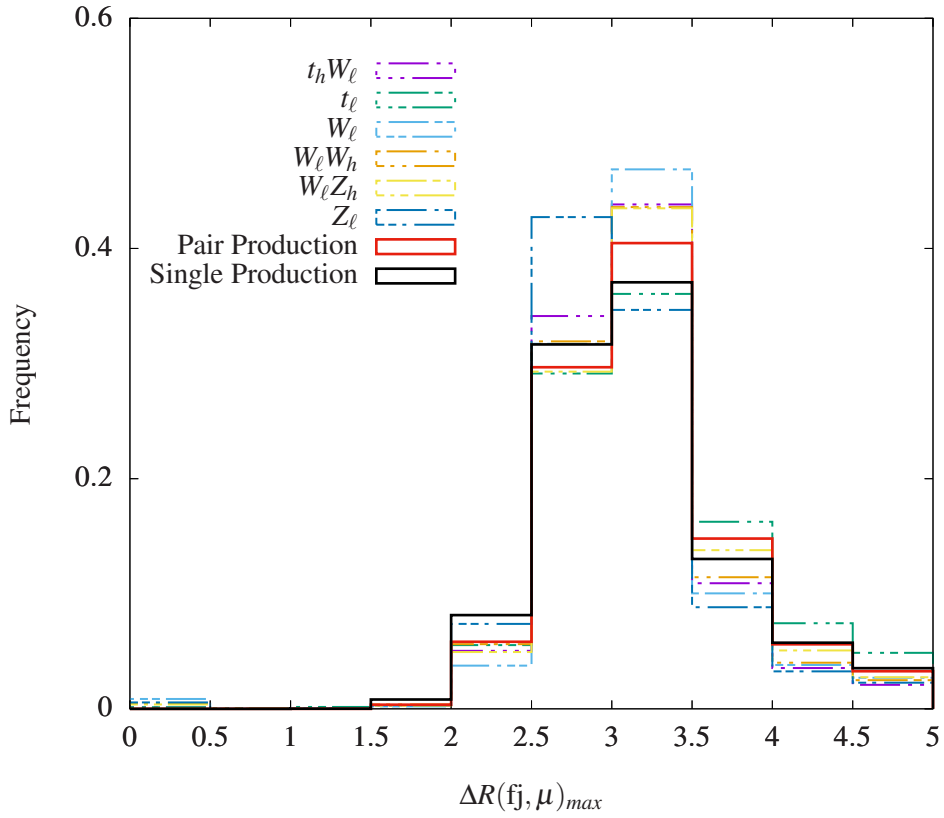

Figure 4.7: $\Delta R(\mathrm{fj}, \mu)$. $M_{\phi_1} = 1250$ GeV/c^2 and $M_{\nu_R} = 500$ GeV/c^2.

distributed in higher momenta bins. Thus, in our selection criteria, we require at least one μ with the following cut:

$$p_T(\mu) > 200 \text{ GeV}/c \tag{4.14}$$

4.3.9 $p_T(j_1)$

We consider the leptoquark decay mode $\phi \to \nu_R + q(j)$. The mass of the leptoquark is in the TeV range, and the mass of RHN (ν_R) is 500 GeV/c^2. The quark (q) produced forms a boosted jet due to the excess energy available. We investigate the presence of such a jet with very high transverse momentum by plotting the highest p_T jet in Fig. 4.9.

We notice that most of the background process events have the highest transverse momentum of their jet in the lower range, and signal events have highly boosted jets. Thus, we require the existence of at least one boosted jet with the following $p_T(j)$ cut:

$$p_T(j_1) > 200 \text{ GeV}/c \tag{4.15}$$

Note that we use j_1 to denote that only one jet per event is required to pass the threshold.

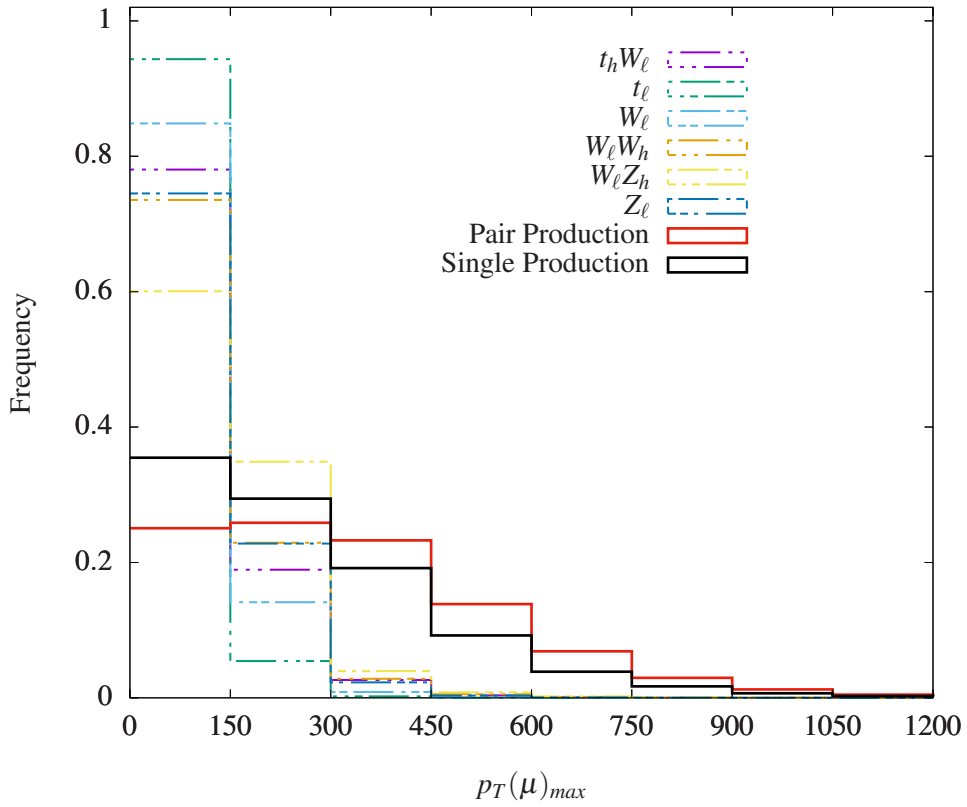

Figure 4.8: Maximum transverse momentum among muons per event. $M_{\phi_1} = 1250$ GeV/c^2 and $M_{\nu_R} = 500$ GeV/c^2.

We also use the same distribution to estimate the appropriate criteria for jet clustering using FASTJET, which requires the minimum acceptable transverse momentum for jets to be included in clustering. This value is better estimated directly in the grid search method. The cut value, denoted by $p_T(\text{fj})$, is set to:

$$p_T(\text{fj}) > 80 \text{ GeV}/c \tag{4.16}$$

4.4 Combining the Cuts

In the previous section, we saw the distribution of the parameters for background and signal events. We also discussed how a few parameters could be correlated, i.e., the same background events lie outside the selection criteria for two cuts. This would result in eliminating a lesser number of events compared to when the distribution was similar, but the parameters were independent.

As the effect of correlation cannot be directly captured while discussing individual cuts, we look at all the cuts simultaneously to achieve the final signal and background events passing the event selection criteria. To improve our reach, we want to increase the significance value $\mathcal{Z}$ as much as possible. Calculation of $\mathcal{Z}$ is discussed in section 4.5. This is the metric we want to optimize by varying the cut

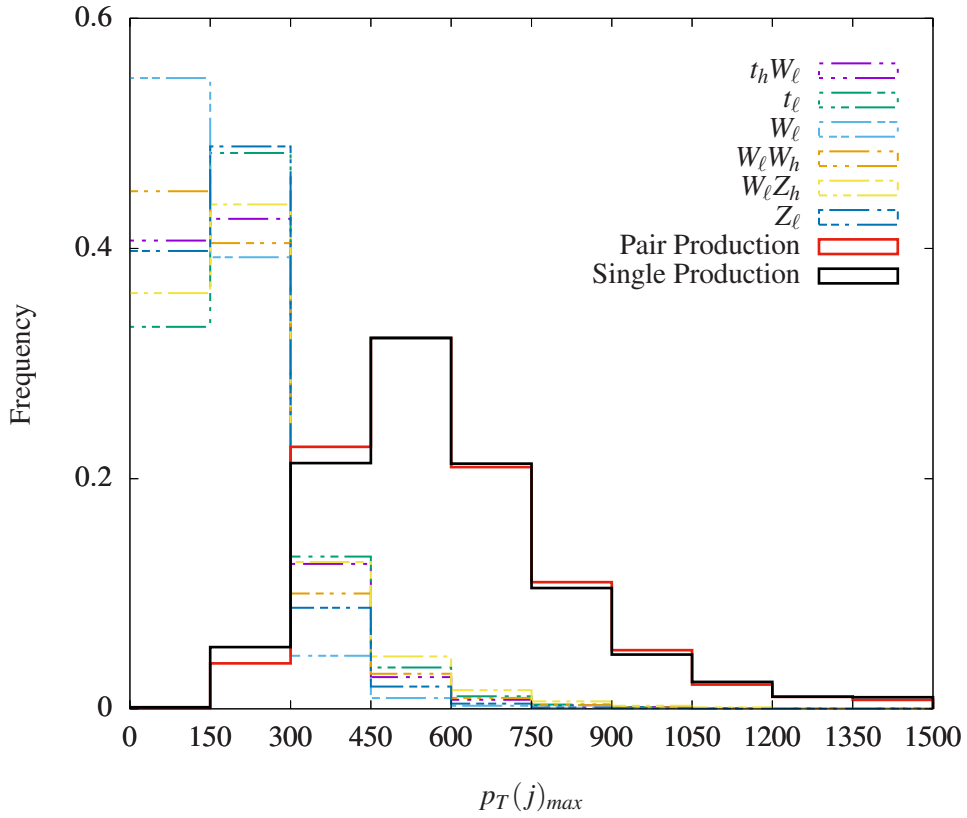

Figure 4.9: Maximum transverse momentum among jets per event. $M_{\phi_1} = 1250$ GeV/c^2 and $M_{\nu_R} = 500$ GeV/c^2.

values. By treating $\mathcal{Z}$ as a function of the above parameters, various methods can be used to find the optimal parameter thresholds which give the highest reach. We use the *grid search* method described below.

4.4.1 Grid Search Method

We can imagine $\mathcal{Z}$ as a continuous function with a 10-dimensional input vector, i.e., in a 10-dimensional space, every point has a scalar value $\mathcal{Z}$, which varies continuously. The dimensions correspond to the above cuts, i.e. $[p_T(\mu),\ p_T(j_1),\ p_T(\text{fj}),\ \tau_{21},\ \tau_{32},\ M(\text{fj}),\ \Delta R(\text{fj},\ \mu),\ S_T,\ \not{E}_T,\ \text{fj}_{HT}]$. The values of the cuts after applying the grid search have been mentioned while discussing the individual cuts, i.e. from eq. 4.7 to eq. 4.16, and in Table 4.2. While various techniques guess what regions are better to look for and then search primarily in those regions, the grid search method divides the space in a grid and searches for all grid points. We discuss the general pros and cons of the grid search method and motivate why we opt for this method.

Pros:

- The entire search space is covered, i.e., the grid search method is exhaustive. This reduces the chances of missing optimal points in case the alternative method skips a few points and outputs a suboptimal point.

- The method is easy to parallelize computationally. Gradient-based and other methods have to wait for the computation of $\mathcal{Z}$ at one point to decide what point to query next. As the grid search method computes $\mathcal{Z}$ for all grid points, it can compute all those in parallel and in any order.

Cons:

- The grid search method requires searching for many more points than the other methods, as there is no prioritization. This is compensated by the ability to parallelize the computation.

- As only points at discrete distances are checked for, it is possible to miss the true optimum, which might not lie on the grid. We do not require such a stringent optimum as our data is a Monte Carlo simulation, and the optimum achieved every time we repeat the experiment can be different. Thus, we do not wish to *overfit* and avoid reporting values that actual experiments at the particle colliders can't achieve. Mass and momentum cuts with values as multiples of 5 and 10 (in GeV/c^2 and GeV/c, respectively) seem reasonable enough.

Thus, the grid search method best fits our use case, so we use it for our experiment.

4.4.2 Cut Flow

We divide the parameters into three categories of cuts to show how the signal is filtered sequentially. $\mathfrak{C}_1$ includes $p_T(\mu)$ cut, $p_T(j_1)$ cut and that no b-tagged jet should be present. $\mathfrak{C}_2$ includes fatjet related parameter cuts like τ_{21}, $M(\text{fj})$, $\Delta R(\text{fj}, \mu)$ and $p_T(\text{fj})$. $\mathfrak{C}_3$ are the scalar cuts, namely, S_T, $\not{E}_T$ and fj_{H_T}. We summarize the values of selection cuts in table 4.2.

4.5 Estimating $\mathcal{Z}$ score

In Ref. [23], it is shown how one could make use of the distribution of the data (rather than just the total number of events) to estimate the signal significance. We follow the method outlined there. After passing the events through the cuts in Table 4.2, we first bin the data by the scalar sum of the transverse momenta of the fatjets, $\text{fj}_{\text{H}_\text{T}}$ (see Fig. 4.10). We then estimate the combined signal significance by Liptak-Stouffer (weighted) $\mathcal{Z}$ score [43, 44]:

$$\mathcal{Z} = \frac{\sum_{i=1}^{5} w_i \mathcal{Z}_i}{\sqrt{\sum_{i=1}^{5} w_i^2}}. \tag{4.17}$$

Selection cuts	Monolepton Channel
$\mathfrak{C}_1$: Selection of high $p_{\rm T}$ Leptons and jets	$p_T(\mu) > 200$ GeV, $p_T(j_1) > 200$ GeV, No b-tagged jet
$\mathfrak{C}_2$: Identification of fatjet	$p_{\rm T}(\text{fj}) > 80$ GeV, $\tau_{21} < 0.3$, $\tau_{32} > 0$, $65 < M(\text{fj}) < 100$ GeV, $\Delta R(\text{fj}, \mu) > 1.0$
$\mathfrak{C}_3$: Scalar cuts	$S_{\rm T} > 1200$ GeV, $\not{E}_T > 150$ GeV, $\text{fj}_{\rm H_T} > 600$ GeV

Table 4.2: The selection cuts applied on the monolepton final states. The b veto reduces the top backgrounds, and fj denotes a fatjet.

■ **Monolepton final state**	Selection cuts		
	$\mathfrak{C}_1$	$\mathfrak{C}_2$	$\mathfrak{C}_3$
Signal benchmarks			
Pair Production. $M_{\phi_1} = 1250$ GeV, $M_{\nu_R} = 500$ GeV	270	126	106
Single Production. $M_{\phi_1} = 1250$ GeV, $M_{\nu_R} = 500$ GeV	291	159	117
		Total number of signal events:	223
Background processes			
$W_\ell\ (+2j)$	4.53×10^7	2.02×10^6	39346
$W_\ell Z_h\ (+2j)$	2.55×10^5	74148	3895
$Z_\ell\ (+2j)$	1.46×10^7	7.93×10^5	2640
$W_\ell W_h\ (+2j)$	2.00×10^5	71229	2483
$t_h W_\ell + t_\ell W_h$	1.52×10^5	45436	1729
$t_\ell + b/j$	3313	555	22
		Total number of background events:	50115

Table 4.3: Cut flows for monolepton final states and the relevant background processes at luminosity $\mathcal{L} = 3$ ab^{-1}.

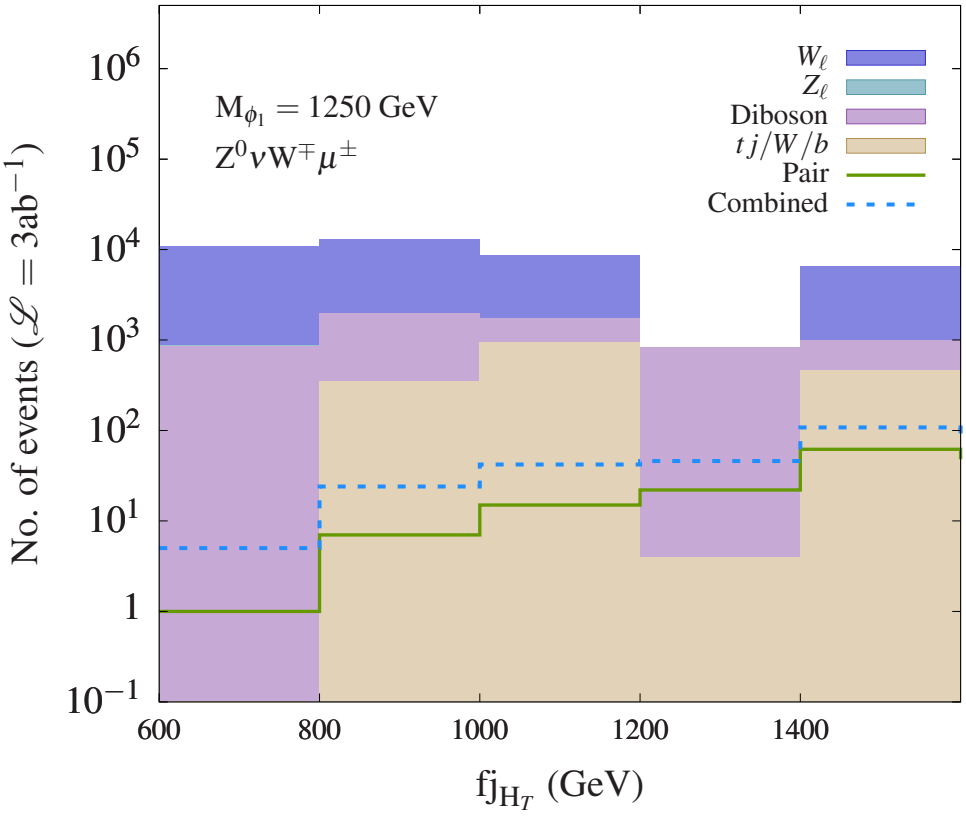

Figure 4.10: The distribution of signal and background events in the monolepton channel. The events are first passed through $\mathfrak{C}_1$–$\mathfrak{C}_3$ (Table 4.2) and then binned according to $\mathrm{fj}_{\mathrm{H_T}}$ (the scalar sum of the transverse momenta of the fatjets). The fifth bin is open on the higher side, i.e., $\mathrm{fj}^{(5)}_{\mathrm{H_T}} > 1400$ GeV. The total number of events for every process is reported in the last row of Table 4.3.

Here, $\mathcal{Z}_i$ is the signal significance score in the i^{th} bin ($i \in \{1, 2, 3, 4, 5\}$) computed as [45]

$$\mathcal{Z}_i = \sqrt{2\left(N_S^i + N_B^i\right) \ln\left(\frac{N_S^i + N_B^i}{N_B^i}\right) - 2N_S^i}\,, \tag{4.18}$$

where the corresponding weight is denoted as w_i, N_S^i (eq. 4.19) and N_B^i (eq. 4.20) are the numbers of signal and background events in the bin:

$$N_S = \Big((\sigma_{pp} \times \epsilon_{pp}) + (\lambda^2 \times \sigma_{sp} \times \epsilon_{sp}) + (\lambda^4 \times \sigma_{\nu_R} \times \epsilon_{\nu_R})\Big) \times L \tag{4.19}$$

$$N_B = \sigma_{bg} \times \epsilon_{bg} \times L \tag{4.20}$$

where σ is the cross-section, ϵ is the efficiency and L is the luminosity. The subscripts pp, sp, ν_R and bg represent pair productions, single productions, RHN pair production (via t - channel LQ) and background process, respectively. The inverse of the variances are generally taken as the weights [46]; we set $w_i^{-1} = (\text{statistical error})^2 = N_B^i$.

Chapter 5

Results

5.1 HL-LHC Prospects

We show the HL-LHC prospects of the monolepton channel for $M_{\nu_R} = 500$ GeV in Fig. 5.1. There we show the 5σ (discovery) and 2σ ($\sim$ exclusion) significance contours on the M_ϕ–λ plane for both ϕ_1 and ϕ_2. We have used the simple models introduced in Sec. 3.1 to estimate the significances at 3 ab^{-1} integrated luminosity; see section 4.5 for our method of estimating the signal significance, $\mathcal{Z}$.

For small values of λ, the 5σ discovery reaches for ϕ_1 and ϕ_2 in the pair production mode in the monolepton channel can go to 0.96 and 0.91 TeV, respectively. But, for $\lambda = 1$, the reaches enhance to 1.08 and 1.01 TeV once the single production and the t-channel RHN-pair production contributions are combined in the signal. For $\lambda = 1$, the actual reaches are slightly better as the $qq \to \nu_R\nu_R$ process also contributes (shown in fig. 5.1). The t-channel processes become important only for large couplings as the contribution by these processes scales as the fourth power of lambda, as mentioned in 3.

The 2σ values provide estimates of the exclusion limits. For $M_{\nu_R} = 500$ GeV, the HL-LHC can exclude up to 1.25 TeV in the cases of both ϕ_1 and ϕ_2.

Note that dilepton channel reaches are higher (> 1.5 TeV for discovery, i.e., 5σ, and 2 TeV for exclusion, i.e., 2σ).

Leptoquark	λ (Coupling)	5σ (Discovery)	2σ (Exclusion)
ϕ_1	$\lambda \approx 0$	0.96	1.08
ϕ_1	$\lambda = 1$	1.08	1.25
ϕ_2	$\lambda \approx 0$	0.91	1.14
ϕ_2	$\lambda = 1$	1.01	1.25

Table 5.1: Discovery and exclusion mass limits (in TeV) for $\lambda = 0, 1$ for ϕ_1 and ϕ_2. $M_{\nu_R} = 500$ GeV.

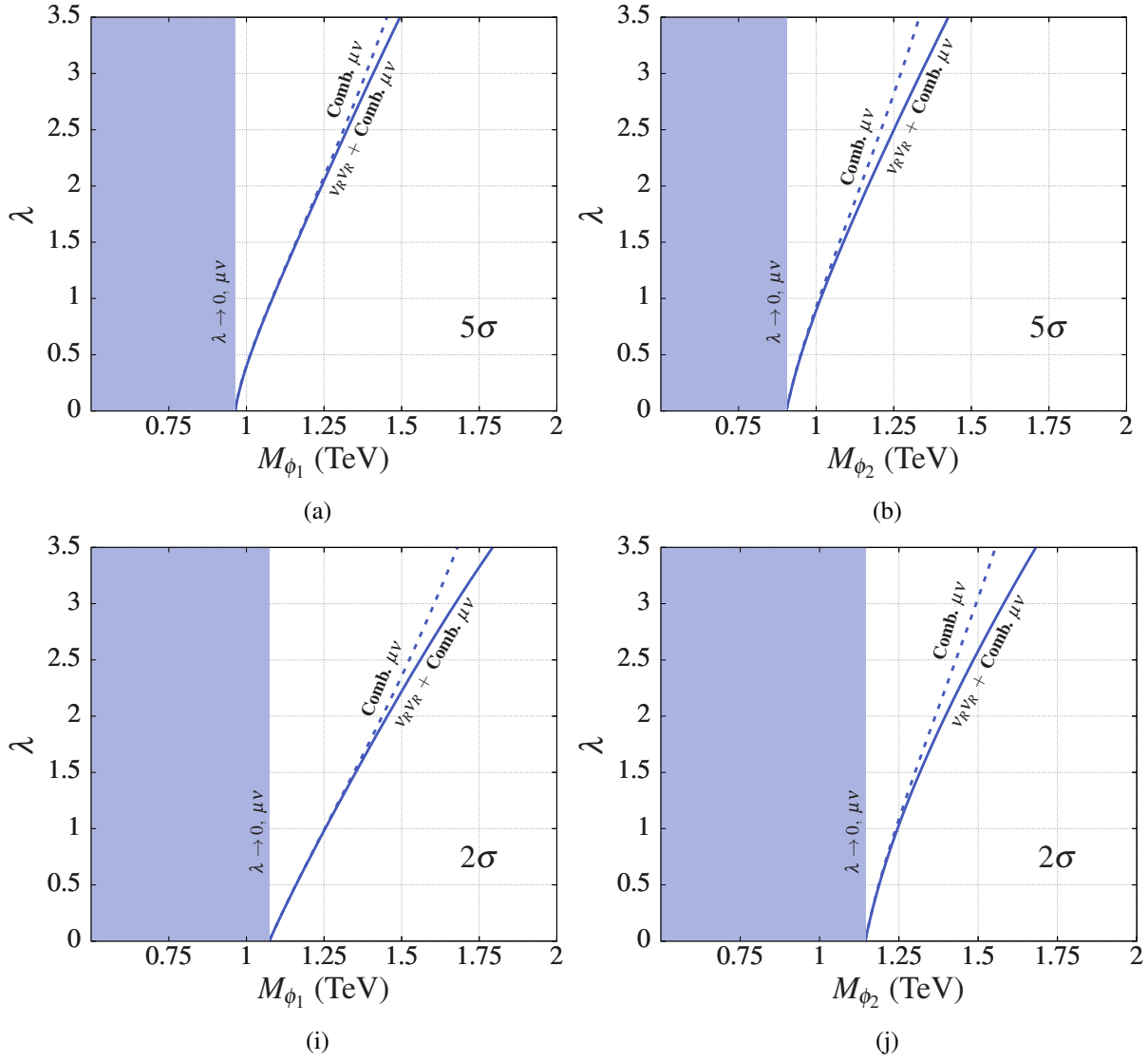

Figure 5.1: The least values of the new coupling λ needed to observe the signals with 5σ (top row) and 2σ (bottom row) significances as functions of masses at the HL-LHC (for monolepton final state). These plots are generated for $M_{\nu_R} = 500$ GeV. The QCD regions ($\lambda \to 0$; LQ pair productions) in the monolepton channel are shown with solid colour; the dashed line is obtained by combining the LQ pair and single production events. Combining single-production events with pair-production events enhances the prospects. However, the prospects improve even further for high couplings since the RHN pair production via LQ exchange also contributes to the signals and enhances the significances (solid lines).

Chapter 6

CaLQ

We have designed an automated LHC-limit calculator for various Leptoquark models to facilitate obtaining indirect bounds on the parameter space of those leptoquarks. We recast the latest LHC high-p_T dilepton search data to obtain precise limits. The alpha version of the package is available at [47].

6.1 Background

We consider the mass and the Yukawa coupling terms in the Lagrangian of leptoquarks as the parameters. Both vector leptoquark couplings (y_χ) and scalar leptoquark couplings (x_ϕ) are 3×3 matrices in flavour space.

$$x^L_\phi / y^L_\chi = \begin{pmatrix} \lambda^L_{11} & \lambda^L_{12} & \lambda^L_{13} \\ \lambda^L_{21} & \lambda^L_{22} & \lambda^L_{23} \\ \lambda^L_{31} & \lambda^L_{32} & \lambda^L_{33} \end{pmatrix}, \quad x^R_\phi / y^R_\chi = \begin{pmatrix} \lambda^R_{11} & \lambda^R_{12} & \lambda^R_{13} \\ \lambda^R_{21} & \lambda^R_{22} & \lambda^R_{23} \\ \lambda^R_{31} & \lambda^R_{32} & \lambda^R_{33} \end{pmatrix}. \tag{6.1}$$

where λ^h_{ab} represents a coupling with a generation quark, b generation lepton with h handedness. Thus, there are eighteen Yukawa coupling terms in the parameter space.

To obtain the indirect bounds, we use the recast run-2 dilepton data (ee, $\mu\mu$ [48], $\tau\tau$ [49]) in terms of the model parameters, $\{\lambda\}$ and $M_{\rm LQ}$. We mimic the experimental analyses (summarised in Ref. [16]) to estimate LQ-signal efficiencies (ϵ's, fractions of signal events surviving the experimental selection cuts) and to populate the experimental distributions with LQ events.

To get the dilepton signal at the LHC from leptoquarks, we consider the single, pair and non-resonant production channels. The numbers of events from single production processes, pair production processes and non-resonant production processes are represented as $\mathcal{N}^s(M_{LQ}, \lambda)$, $\mathcal{N}^p(M_{LQ}, \lambda)$ and $\mathcal{N}^{nr}(M_{LQ}, \lambda)$ respectively. Each of $\mathcal{N}^s, \mathcal{N}^p$ and $\mathcal{N}^{nr}$ can be represented as:

$$\mathcal{N} = L \times \mathcal{B}(M_{LQ}, \lambda_1, \ldots, \lambda_k) \times \sum_{1 \le i,j \le k} P(\lambda_i, \lambda_j) \times \sigma_{ij}(M_{LQ}) \times \epsilon(M_{LQ}) \tag{6.2}$$

where k couplings are being considered, $P(\lambda_i, \lambda_j) = \lambda_i^n * \lambda_j^m$ for some n and m, $\sigma_{ij}(M_{LQ})$ is the process related cross-section, $\mathcal{B}(M_{LQ}, \lambda_1, \ldots, \lambda_k)$ is the branching fraction, $\epsilon(M_{LQ})$ is the efficiency and L is the luminosity. Note that only P and $\mathcal{B}$ have λ - dependence.

6.2 Overview of χ^2 Test

In order to recast the LHC dilepton search data, we perform a χ^2 test to estimate the limits on the parameters of our LQ model from the transverse mass distribution in case of $\tau\tau$ and the invariant mass distributions for ee and $\mu\mu$. We briefly mention the steps we followed to obtain the χ^2 and $\Delta\chi^2$ values. For more details, refer to the appendix of [16]. We use the same notation as mentioned there.
The χ^2 value, which is a function of the leptoquark mass, M_{LQ}, and the Yukawa coupling terms, λ, is defined as:

$$\chi^2(M_{LQ},\lambda) = \sum_i \left(\frac{\mathcal{N}_{\rm T}^i(M_{LQ},\lambda) - \mathcal{N}_{\rm D}^i}{\Delta\mathcal{N}^i} \right)^2 \tag{6.3}$$

where the sum runs over the number of bins. $\mathcal{N}_{\rm T}^i(M_{LQ},\lambda) \equiv$ expected theory events in the i^{th} bin. Thus,

$$\begin{aligned} \mathcal{N}_{\rm T}^i(M_{LQ},\lambda) &= \mathcal{N}_{LQ}^i(M_{LQ},\lambda) + \mathcal{N}_{\rm SM}^i \\ &= \left[\mathcal{N}^p(M_{LQ},\lambda) + \mathcal{N}^s(M_{LQ},\lambda) + \mathcal{N}^{nr}(M_{LQ},\lambda)\right] + \mathcal{N}_{\rm SM}^i. \end{aligned} \tag{6.4}$$

where $\mathcal{N}_{\rm SM} \equiv$ Total signal events from the SM background.
$\mathcal{N}_{\rm D} \equiv$ Total number of observed events.

The error $\Delta\mathcal{N} = \sqrt{(\Delta\mathcal{N}_{stat})^2 + (\Delta\mathcal{N}_{syst})^2}$. where $\Delta\mathcal{N}_{stat} = \sqrt{\mathcal{N}_D}$ and we assume a uniform 10% systematic error, i.e., $\Delta\mathcal{N}_{syst} = \delta \times \mathcal{N}_D$ with $\delta = 0.1$. Given the lambda (coupling terms) and

Bins	$\mathcal{N}_D$	$\mathcal{N}_{SM}$	$\mathcal{N}^p$	$\mathcal{N}^s$	$\mathcal{N}^{nr}$	$\mathcal{N}_{LQ} = \mathcal{N}^p + \mathcal{N}^s + \mathcal{N}^{nr}$	$\mathcal{N}'_{bin} = \frac{(\mathcal{N}_{LQ}+\mathcal{N}_{SM}-\mathcal{N}_D)^2}{\mathcal{N}_D+(0.1*\mathcal{N}_D)^2}$
⋮							⋮
							$\chi^2 = \sum_i \mathcal{N}'_{bin}$

Table 6.1: χ^2 contingency table

mass dependence of each cell in Table 6.1, naively, one would have to compute the value of every cell in the table to obtain the χ^2 value for each given λ. We call this the tabular method. We need to find χ^2_{min} and the corresponding λ^* such that χ^2_{min} is the least value that χ^2 obtains in the valid parameter region. In such a scenario, the grid search method has to be used where grid points at equal intervals in the valid parameter space are tested. If the number of couplings that are switched on is n and per coupling m intervals are tested, the complexity of the computation is $\mathcal{O}(m^n)$, i.e., exponential in the number of couplings. Thus, this methodology is infeasible when the number of coupling (which can go up to 18) goes beyond 5. If the number of intervals is decreased to reduce computation, the possibility of missing the true minima increases. This indicates the need for a better approach to solving this problem.

6.3 Viewing χ^2 as a Polynomial in $\lambda_i s$

We notice that $\mathcal{N}_{SM}$ and $\mathcal{N}_D$ (and consequently, $\Delta\mathcal{N}$) are independent of $\lambda_i s$ in eq. 6.3. Only $\mathcal{N}^s$, $\mathcal{N}^p$, $\mathcal{N}^{nr}$, and therefore, $\mathcal{N}_T$, are λ_i dependent terms. More specifically, they are multivariate polynomials [1] in the coupling terms $\lambda_i s$. As only $\mathcal{N}_D$ appears in the denominator of χ^2, the denominator is constant per table. The numerator in each bin, however, is the square of a linear combination of various multivariate polynomials in different $\lambda_i s$, i.e., $(\mathcal{N}^s + \mathcal{N}^p + \mathcal{N}^{nr} + \mathcal{N}_{SM} - \mathcal{N}_D)^2$. This itself is a multivariate polynomial in λ_i.

For example, χ^2, when only two couplings (λ_1 and λ_2) are considered, will be as follows:

$$\begin{aligned}\chi^2(\lambda_1,\lambda_2) = c_{00} + c_{10}\lambda_1^2 + c_{01}\lambda_2^2 + c_{20}\lambda_1^4 + c_{02}\lambda_2^4 + c_{30}\lambda_1^6 + c_{03}\lambda_2^6 + c_{40}\lambda_1^8 + c_{04}\lambda_2^8 \\ + c_{11}\lambda_1^2\lambda_2^2 + c_{21}\lambda_1^4\lambda_2^2 + c_{12}\lambda_1^2\lambda_2^4 + c_{22}\lambda_1^4\lambda_2^4 + c_{31}\lambda_1^6\lambda_2^2 + c_{13}\lambda_1^2\lambda_2^6 \end{aligned} \tag{6.5}$$

where the products of cross-section, branching fraction, luminosity and efficiency have been reduced to coefficients c_{ij} of the corresponding terms, i.e., $c_{ij} = c_{ij}(M_{LQ}, L)$.

Once we compute all the coefficients of the polynomial, χ^2 for any value of $\lambda_i s$ can be computed just by substitution in the polynomial. Thus, the χ^2 value computation is reduced to the equivalent of one row's worth of computation in the tabular method.

6.4 Using the Polynomial form to obtain χ^2_{min}

To obtain χ^2_{min} and 2σ limits, we can either proceed to use the polynomial form to use the grid search method (i.e. checking the χ^2 value after small intervals) or we can exploit the polynomial method further. As we have the explicit polynomial form, we can compute the derivatives (gradient, hessian, etc.). Thus, we can now use the class of minimization techniques which require these derivatives. In Gradient Descent, we start at a particular $(\Lambda_0) = (\lambda_i, \ldots, \lambda_n)_0$, compute the gradient $\mathcal{G}$ at the current point and find a new point in the opposite direction of the gradient. This process is repeated till a minimum is reached. We can go further to use the second derivative too, by using the Newton-Raphson method. As we have multiple λ_is, the gradient is a vector, and the second derivative, the Hessian, is a matrix.

$$\text{Gradient } \mathcal{G}\text{: } \begin{bmatrix} \frac{\partial\chi^2}{\partial\lambda_1} \\ \vdots \\ \frac{\partial\chi^2}{\partial\lambda_n} \end{bmatrix} \qquad \text{Hessian } \mathcal{H}\text{: } \begin{bmatrix} \frac{\partial^2\chi^2}{\partial\lambda_1\partial\lambda_1} & \cdots & \frac{\partial^2\chi^2}{\partial\lambda_1\partial\lambda_n} \\ \vdots & \ddots & \vdots \\ \frac{\partial^2\chi^2}{\partial\lambda_n\partial\lambda_1} & \cdots & \frac{\partial^2\chi^2}{\partial\lambda_n\partial\lambda_n} \end{bmatrix}$$

In Newton's method, we perform the following iteration:

$$x_{k+1} = x_k - \mathcal{H}^{-1}\mathcal{G}$$

[1] ignoring the λ_i dependence of $\mathcal{B}$, the branching fraction, for ease of exposition. If the λ - dependence of $\mathcal{B}$ is considered, the form of χ^2 becomes a rational polynomial, but the method remains valid.

where x_k represents the approximate minimum achieved in the k^{th} iteration and $\mathcal{H}^{-1}$ represents the inverse of the Hessian. The inverse can be computed either in the polynomial form, or the numerical value of Hessian can be calculated to use it to compute the inverse. Following is the Python code for Newton's Method:

```
import numpy as np
def newtons_method(initial_l1, initial_l2, epoch):
    x = np.array([initial_l1, initial_l2])
    # Here initial_l1 refers to the initial value of lambda_1.
    while(epoch):
        epoch = epoch - 1
        x = x - np.matmul(Hinv(x), Grad(x))
        # Hinv is the inverse of the Hessian and Grad is the gradient
    return x
```

Here epoch is the number of iterations desired. Typically, this algorithm converges to a minimum in a very small number of iterations (<100) as opposed to gradient descent (>10000) in two λ scenarios (i.e. $n = 2$). The returned value of x gives us the value of the $\Lambda^* = (\lambda_1^*, \ldots, \lambda_n^*)$ for χ^2_{min}[2]. χ^2_{min} can be obtained by direct substitution of λ_i^* in the polynomial form[3]. The degree of $\chi^2()$ polynomial is generally high; thus, there will be multiple local minima. One method to find the global minimum would be to repeat the process multiple times with different starting points and choose the best χ^2_{min} achieved.

6.5 Code

In practice, computing Hessian symbolically for more than four λ_i is quite time-consuming [4]. We convert the symbolic function of $\chi^2()$ to a Python lambda function, which is much faster in computing the value at particular Λ. We tested *SciPy* (library by Python for scientific computing) for minimization and found them to be faster than our implementation of the Newton-Raphson method (with the bottle-neck being computation of Hessian symbolically). All methods provided by *scipy.optimize* performed similarly. In the CaLQ code, we compute the minimum using the *Nealder-Mead* method and *BFGS* algorithm provided by scipy. Nealder-Mead does non-linear optimizations, and BFGS approximates the Hessian matrix and uses it without inverting it, reducing the complexity to $\mathcal{O}(n^2)$ as opposed to $\mathcal{O}(n^3)$ of our standard Newton's method implementation.

As mentioned above, the alpha version of CaLQ is available at [47]. A user manual is available as a *Readme* file. It includes the installation instructions, different commands available to vary parameters,

[2] That is, $x[0] = \lambda_1^*, x[1] = \lambda_2^*, \ldots, x[n] = \lambda_n^*$.
[3] λ^* represents the values of $\lambda_i s$ at χ^2_{min}
[4] especially due to χ^2 being a rational function if $\mathcal{B}$ is a rational function.

usage in the interactive mode, usage in the non-interactive mode and how to extend the calculator to include more leptoquark models.

Chapter 7

Summary and Conclusions

In this thesis, we discuss the discovery prospects of scalar LQs decaying exclusively to second-generation quarks and right-handed neutrinos. LQs, because of their simultaneous coupling to quarks and leptons, are one of the promising candidates to explain the anomalies in B-physics. Observing RHN could be the key to understanding neutrino mass generation. We probe the LQ-induced production of RHNs and their subsequent decay. RHNs can be produced copiously if their mass is smaller than the LQs. Once produced, RHNs can decay to a W boson and a charged lepton, or, a Z boson and a light neutrino. RHNs can be produced in three different ways. A pair of resonantly produced LQs or a single LQ produced along with a RHN and a quark can give a pair of RHNs. There is another non-resonant mode in which a pair of RHNs are produced via t- channel LQ exchange. Once a pair of RHNs are produced, we study the monolepton decay channel, i.e., one RHN decaying to a W boson and a muon and the other decaying to a Z boson and a light neutrino. Both the W boson and Z boson are considered to decay hadronically. The monolepton channel is more challenging to analyze as it is difficult to reconstruct neutrinos. Our selection criteria allow us to combine events from all three RHN production modes. For conservative estimates, we have focussed mainly on the second-generation decay of RHNs. Thus, our signal contains a single muon and hadronically decaying gauge bosons. Our cut optimization techniques involve analyzing the cuts individually and incorporating a grid search method to obtain the best combination of cut values, with the goal of enhancing signal efficiency. In order to give a quantitative picture of the results from our search strategy, we give 5σ and 2σ significance contours.

Apart from the above work, we also presented a methodology to reduce computations required to compute functions on contingency tables in the context of Leptoquark couplings in chapter 6. The polynomial method enables using line search methods to find special points like minima and maxima. We use this method to design a leptoquark limit calculator for obtaining indirect bounds on the parameter space of various leptoquarks [47]. However, this methodology can be used wherever a function on a table (which contains variable elements in its cells) can be reduced to a polynomial.

Publications and Patents

1. **Right-handed neutrino pair production via second-generation leptoquarks**
   Arvind Bhaskar, Yash Chaurasia, Kuldeep Deka, Tanumoy Mandal, Subhadip Mitra, Ananya Mukherjee
   arXiv:2301.11889
   DOI: 10.1016/j.physletb.2023.138039

2. **PUPoW: A framework for designing blockchains with practically-useful-proof-of-work & VanityCoin**
   Yash Chaurasia, Visvesh Subramanian, Sujit Gujar
   2021 IEEE International Conference on Blockchain, Melbourne, Australia, 2021, pp. 122-129
   arXiv:2210.06738
   DOI: 10.1109/Blockchain53845.2021.00026

3. **CaLQ: LHC-limit calculator for Leptoquark models** (in progress)
   Arvind Bhaskar, Yash Chaurasia, Atirek Kumar, Tanumoy Mandal, Subhadip Mitra
   github.com/rsrchtsm/iCaLQ

4. **System And Method For Better Utilization Of Power Consumption In Blockchain System By Validating Digital Currency Transactions With Minimal Computing Resources** (patent)
   Sujit Prakash Gujar, Yash Chaurasia, Visvesh Subramanian
   USPTO Application Number: 18/115,693

Bibliography

[1] W. N. Cottingham and D. A. Greenwood. *An introduction to the standard model of particle physics*. Cambridge University Press, Apr. 2007, pp. 50–52. ISBN: 978-0-511-27136-6, 978-0-521-85249-4.

[2] I. Béjar Alonso et al. "High-Luminosity Large Hadron Collider (HL-LHC): Technical design report". In: *CERN Yellow Reports* 10 (Dec. 2020). DOI: 10.23731/CYRM-2020-0010. URL: https://doi.org/10.23731/CYRM-2020-0010.

[3] Shankha Banerjee et al. "Prospects of Heavy Neutrino Searches at Future Lepton Colliders". In: *Phys. Rev. D* 92 (2015), p. 075002. DOI: 10.1103/PhysRevD.92.075002. arXiv: 1503.05491 [hep-ph].

[4] Arindam Das and Nobuchika Okada. "Inverse seesaw neutrino signatures at the LHC and ILC". In: *Phys. Rev. D* 88 (2013), p. 113001. DOI: 10.1103/PhysRevD.88.113001. arXiv: 1207.3734 [hep-ph].

[5] Arindam Das and Nobuchika Okada. "Bounds on heavy Majorana neutrinos in type-I seesaw and implications for collider searches". In: *Phys. Lett. B* 774 (2017), pp. 32–40. DOI: 10.1016/j.physletb.2017.09.042. arXiv: 1702.04668 [hep-ph].

[6] Ujjal Kumar Dey et al. "Searching for Leptoquarks at IceCube and the LHC". In: *Phys. Rev. D* 98.3 (2018), p. 035014. DOI: 10.1103/PhysRevD.98.035014. arXiv: 1709.02009 [hep-ph].

[7] Priyotosh Bandyopadhyay and Rusa Mandal. "Revisiting scalar leptoquark at the LHC". In: *Eur. Phys. J. C* 78 (2018), p. 491. DOI: 10.1140/epjc/s10052-018-5959-x. arXiv: 1801.04253 [hep-ph].

[8] Arindam Das et al. "Probing right handed neutrinos at the LHeC and lepton colliders using fat jet signatures". In: *Phys. Rev. D* 99.5 (2019), p. 055030. DOI: 10.1103/PhysRevD.99.055030. arXiv: 1811.04291 [hep-ph].

[9] Kushagra Chandak, Tanumoy Mandal, and Subhadip Mitra. "Hunting for scalar leptoquarks with boosted tops and light leptons". In: *Phys. Rev. D* 100.7 (2019), p. 075019. DOI: 10.1103/PhysRevD.100.075019. arXiv: 1907.11194 [hep-ph].

[10] Rojalin Padhan et al. "Signatures of $\tilde{R}_2$ class of Leptoquarks at the upcoming ep colliders". In: *Phys. Rev. D* 101.7 (2020), p. 075037. DOI: 10.1103/PhysRevD.101.075037. arXiv: 1912.07236 [hep-ph].

[11] Arvind Bhaskar, Tanumoy Mandal, and Subhadip Mitra. "Boosting vector leptoquark searches with boosted tops". In: *Phys. Rev. D* 101.11 (2020), p. 115015. DOI: 10.1103/PhysRevD.101.115015. arXiv: 2004.01096 [hep-ph].

[12] Nivedita Ghosh, Santosh Kumar Rai, and Tousik Samui. "Collider Signatures of a Scalar Leptoquark and Vector-like Lepton in Light of Muon Anomaly". In: *arXiv* (June 2022). arXiv: 2206.11718 [hep-ph].

[13] Nishita Desai and Amartya Sengupta. "Status of leptoquark models after LHC Run-2 and discovery prospects at future colliders". In: *arXiv* (Jan. 2023). arXiv: 2301.01754 [hep-ph].

[14] Georges Aad et al. "Search for pairs of scalar leptoquarks decaying into quarks and electrons or muons in $\sqrt{s}$ = 13 TeV pp collisions with the ATLAS detector". In: *JHEP* 10 (2020), p. 112. DOI: 10.1007/JHEP10(2020)112. arXiv: 2006.05872 [hep-ex].

[15] Tanumoy Mandal, Subhadip Mitra, and Swapnil Raz. "$R_{D^{(*)}}$ motivated $\mathcal{S}_1$ leptoquark scenarios: Impact of interference on the exclusion limits from LHC data". In: *Phys. Rev. D* 99.5 (2019), p. 055028. DOI: 10.1103/PhysRevD.99.055028. arXiv: 1811.03561 [hep-ph].

[16] Arvind Bhaskar et al. "Precise limits on the charge-2/3 U1 vector leptoquark". In: *Phys. Rev. D* 104.3 (2021), p. 035016. DOI: 10.1103/PhysRevD.104.035016. arXiv: 2101.12069 [hep-ph].

[17] Debottam Das et al. "Probing sterile neutrinos in the framework of inverse seesaw mechanism through leptoquark productions". In: *Phys. Rev. D* 97.1 (2018), p. 015024. DOI: 10.1103/PhysRevD.97.015024. arXiv: 1708.06206 [hep-ph].

[18] Sanjoy Mandal, Manimala Mitra, and Nita Sinha. "Probing leptoquarks and heavy neutrinos at the LHeC". In: *Phys. Rev. D* 98.9 (2018), p. 095004. DOI: 10.1103/PhysRevD.98.095004. arXiv: 1807.06455 [hep-ph].

[19] Arvind Bhaskar et al. "Enhancing scalar productions with leptoquarks at the LHC". In: *Phys. Rev. D* 102.3 (2020), p. 035002. DOI: 10.1103/PhysRevD.102.035002. arXiv: 2002.12571 [hep-ph].

[20] Giovanna Cottin et al. "Displaced neutrino jets at the LHeC". In: *JHEP* 06 (2022), p. 168. DOI: 10.1007/JHEP06(2022)168. arXiv: 2104.13578 [hep-ph].

[21] Arvind Bhaskar et al. "Leptoquark-assisted singlet-mediated di-Higgs production at the LHC". In: *Phys. Lett. B* 833 (2022), p. 137341. DOI: 10.1016/j.physletb.2022.137341. arXiv: 2205.12210 [hep-ph].

[22] I. Doršner et al. "Physics of leptoquarks in precision experiments and at particle colliders". In: *Phys. Rept.* 641 (2016), pp. 1–68. DOI: 10.1016/j.physrep.2016.06.001. arXiv: 1603.04993 [hep-ph].

[23] Arvind Bhaskar et al. “Improving third-generation leptoquark searches with combined signals and boosted top quarks”. In: *Phys. Rev. D* 104.7 (2021), p. 075037. DOI: 10.1103/PhysRevD.104.075037. arXiv: 2106.07605 [hep-ph].

[24] Adam Alloul et al. “FeynRules 2.0 - A complete toolbox for tree-level phenomenology”. In: *Comput. Phys. Commun.* 185 (2014), pp. 2250–2300. DOI: 10.1016/j.cpc.2014.04.012. arXiv: 1310.1921 [hep-ph].

[25] Celine Degrande et al. “UFO - The Universal FeynRules Output”. In: *Comput. Phys. Commun.* 183 (2012), pp. 1201–1214. DOI: 10.1016/j.cpc.2012.01.022. arXiv: 1108.2040 [hep-ph].

[26] J. Alwall et al. “The automated computation of tree-level and next-to-leading order differential cross sections, and their matching to parton shower simulations”. In: *JHEP* 07 (2014), p. 079. DOI: 10.1007/JHEP07(2014)079. arXiv: 1405.0301 [hep-ph].

[27] M. Kramer et al. “Pair production of scalar leptoquarks at the CERN LHC”. In: *Phys. Rev. D* 71 (2005), p. 057503. DOI: 10.1103/PhysRevD.71.057503. arXiv: hep-ph/0411038.

[28] Tanumoy Mandal, Subhadip Mitra, and Satyajit Seth. “Pair Production of Scalar Leptoquarks at the LHC to NLO Parton Shower Accuracy”. In: *Phys. Rev. D* 93.3 (2016), p. 035018. DOI: 10.1103/PhysRevD.93.035018. arXiv: 1506.07369 [hep-ph].

[29] Christoph Borschensky et al. “Scalar leptoquarks at the LHC and flavour anomalies: a comparison of pair-production modes at NLO-QCD”. In: *JHEP* 11 (2022), p. 006. DOI: 10.1007/JHEP11(2022)006. arXiv: 2207.02879 [hep-ph].

[30] Torbjörn Sjöstrand et al. “An introduction to PYTHIA 8.2”. In: *Comput. Phys. Commun.* 191 (2015), pp. 159–177. DOI: 10.1016/j.cpc.2015.01.024. arXiv: 1410.3012 [hep-ph].

[31] J. de Favereau et al. “DELPHES 3, A modular framework for fast simulation of a generic collider experiment”. In: *JHEP* 02 (2014), p. 057. DOI: 10.1007/JHEP02(2014)057. arXiv: 1307.6346 [hep-ex].

[32] Matteo Cacciari, Gavin P. Salam, and Gregory Soyez. “The anti-k_t jet clustering algorithm”. In: *JHEP* 04 (2008), p. 063. DOI: 10.1088/1126-6708/2008/04/063. arXiv: 0802.1189 [hep-ph].

[33] Matteo Cacciari, Gavin P. Salam, and Gregory Soyez. “FastJet User Manual”. In: *Eur. Phys. J. C* 72 (2012), p. 1896. DOI: 10.1140/epjc/s10052-012-1896-2. arXiv: 1111.6097 [hep-ph].

[34] Tanumoy Mandal and Subhadip Mitra. “Probing Color Octet Electrons at the LHC”. In: *Phys. Rev. D* 87.9 (2013), p. 095008. DOI: 10.1103/PhysRevD.87.095008. arXiv: 1211.6394 [hep-ph].

[35] Tanumoy Mandal, Subhadip Mitra, and Satyajit Seth. "Single Productions of Colored Particles at the LHC: An Example with Scalar Leptoquarks". In: *JHEP* 07 (2015), p. 028. DOI: 10.1007/JHEP07(2015)028. arXiv: 1503.04689 [hep-ph].

[36] Tanumoy Mandal, Subhadip Mitra, and Satyajit Seth. "Probing Compositeness with the CMS $eejj$ & eej Data". In: *Phys. Lett. B* 758 (2016), pp. 219–225. DOI: 10.1016/j.physletb.2016.05.020. arXiv: 1602.01273 [hep-ph].

[37] Arvind Bhaskar et al. "Right-handed neutrino pair production via second-generation leptoquarks". In: (Jan. 2023). arXiv: 2301.11889 [hep-ph].

[38] Stefano Catani et al. "Vector boson production at hadron colliders: a fully exclusive QCD calculation at NNLO". In: *Phys. Rev. Lett.* 103 (2009), p. 082001. DOI: 10.1103/PhysRevLett.103.082001. arXiv: 0903.2120 [hep-ph].

[39] Giovanni Balossini et al. "Combination of electroweak and QCD corrections to single W production at the Fermilab Tevatron and the CERN LHC". In: *JHEP* 01 (2010), p. 013. DOI: 10.1007/JHEP01(2010)013. arXiv: 0907.0276 [hep-ph].

[40] John M. Campbell, R. Keith Ellis, and Ciaran Williams. "Vector boson pair production at the LHC". In: *JHEP* 07 (2011), p. 018. DOI: 10.1007/JHEP07(2011)018. arXiv: 1105.0020 [hep-ph].

[41] Nikolaos Kidonakis. "Theoretical results for electroweak-boson and single-top production". In: *PoS* DIS2015 (2015), p. 170. DOI: 10.22323/1.247.0170. arXiv: 1506.04072 [hep-ph].

[42] Jesse Thaler and Ken Van Tilburg. "Identifying boosted objects with N-subjettiness". In: *Journal of High Energy Physics* 2011.3 (Mar. 2011). DOI: 10.1007/jhep03(2011)015. URL: https://doi.org/10.1007%2Fjhep03%282011%29015.

[43] S. A. Stouffer et al. *The American Soldier, Vol.1: Adjustment during Army Life*. Princeton: Princeton University Press, 1949.

[44] Tamás Lipták. "On the combination of independent tests". In: *Magyar Tud Akad Mat Kutato Int Kozl* 3 (1958), pp. 171–197.

[45] Glen Cowan et al. "Asymptotic formulae for likelihood-based tests of new physics". In: *Eur. Phys. J. C* 71 (2011). [Erratum: Eur.Phys.J.C 73, 2501 (2013)], p. 1554. DOI: 10.1140/epjc/s10052-011-1554-0. arXiv: 1007.1727 [physics.data-an].

[46] M. C. Whitlock. "Combining probability from independent tests: the weighted Z-method is superior to Fisher's approach". In: *Journal of Evolutionary Biology* 18.5 (2005), pp. 1368–1373. DOI: https://doi.org/10.1111/j.1420-9101.2005.00917.x. URL: https://onlinelibrary.wiley.com/doi/abs/10.1111/j.1420-9101.2005.00917.x.

[47] Arvind Bhaskar et al. *CaLQ*. https://github.com/rsrchtsm/iCaLQ. 2022.

[48] Albert M Sirunyan et al. "Search for resonant and nonresonant new phenomena in high-mass dilepton final states at $\sqrt{s} = 13$ TeV". In: *JHEP* (Mar. 2021). **HEPData** link: https://www.hepdata.net/record/ins1849964. arXiv: 2103.02708 [hep-ex].

[49] Georges Aad et al. "Search for heavy Higgs bosons decaying into two tau leptons with the ATLAS detector using pp collisions at $\sqrt{s} = 13$ TeV". In: *Phys. Rev. Lett.* 125.5 (2020). **HEPData** link: https://www.hepdata.net/record/ins1782650., p. 051801. DOI: 10.1103/PhysRevLett.125.051801. arXiv: 2002.12223 [hep-ex].